Kinetic energy equipartition: A tool to characterize quantum thermalization

Carlos F. Destefani [*] and Xavier Oriols [†]

Department of Electronic Engineering, Universitat Autònoma de Barcelona, 08193 Bellaterra, Barcelona, Spain

According to both Bohmian and stochastic quantum mechanics, the standard quantum mechanical kinetic energy can be understood as consisting of two hidden-variable components. One component is associated with the current (or Bohmian) velocity, while the other is associated with the osmotic velocity (or quantum potential), and they are identified with the phase and the amplitude, respectively, of the wave function. These two components are experimentally accessible through the real and imaginary parts of the weak value of the momentum postselected in position. In this paper, a kinetic energy equipartition is presented as a signature of quantum thermalization in closed systems. This means that the expectation value of the standard kinetic energy is equally shared between the expectation values of the squares of these two hidden-variable components. Such components cannot be reached from expectation values linked to typical Hermitian operators. To illustrate these concepts, numerical results for the nonequilibrium dynamics of a few-particle harmonic trap under random disorder are presented. Furthermore, the advantages of using the center-of-mass frame of reference for dealing with systems containing many indistinguishable particles are also discussed.

I. INTRODUCTION

A renewed interest in statistical mechanics of closed quantum systems has arisen [1–15] as a consequence of the successful experimental ability to isolate and manipulate bosonic [16–20] and fermionic [21–25] many-body systems built on ultracold atomic gases subjected to optical lattices. The main question to be addressed is when an initial nonequilibrium state thermalizes and, if so, under which conditions. The eigenstate thermalization hypothesis (ETH) [26,27], which has become a cornerstone in the study of quantum thermalization, claims that all relevant energy eigenstates of a given Hamiltonian, in the description of a quantum state, are thermal in the sense that they are similar to an equilibrium state as long as one deals with macroscopic observables. In recent years a large number of numerical experiments have successfully tested the ETH by directly diagonalizing in physical space some sort of short-range many-body lattice Hamiltonian, such as a Fermi- or Bose-Hubbard Hamiltonian [17,22,23,28–30] and an XXZ- or XYZ-Heisenberg Hamiltonian [6,15,18,31–34], in the search for chaotic signatures in the statistics of their spectra, as in general induced by local impurities, without the need to explicitly evolve the initial nonequilibrium state. The true time evolution of such a state is not as widespread due to the inherently huge configuration space involved.

Our understanding of quantum thermalization has largely been based on expectation values of observables linked to Hermitian operators. It is well known that other explanations of quantum phenomena allow one to discuss properties not directly linked to Hermitian operators. Such alternative explanations are in general labeled as hidden-variable theories. The Bohmian theory, formulated by de Broglie in 1927 [35] and further developed by Bohm in 1952 [36], is the most well-known example of a quantum theory with additional microscopic variables: Particles have always well-defined positions that conform trajectories. Another example is the stochastic quantum mechanics, proposed by Nelson in 1966 [37]; although it also assumes particles with well-defined trajectories, these are unknown, and only their statistical behavior is handled.

These two hidden-variable theories assume that the standard quantum mechanical kinetic energy, which is labeled in this paper as the orthodox kinetic energy, in fact has two components: In the Bohmian theory, it is computed as the square of the so-called Bohmian velocity plus a quantum potential, while in the stochastic quantum mechanics, it is given by the square of a mean current velocity plus the square of a so-called osmotic velocity. The central question in this paper is whether these two hidden-variable components of the kinetic energy also thermalize when the orthodox kinetic energy thermalizes. We show that in fact, one can characterize the thermalization time t_{eq} as the time when the expectation values of the (squared) current and osmotic velocities become equal or, similarly, when the expectation values of the Bohmian kinetic and quantum potential energies become the same, each being equal to half of the orthodox kinetic energy. Such a *kinetic energy equipartition* is the hidden-variable signature of quantum thermalization.

Nowadays, the information carried by such hidden variables is accessible in the laboratory through the so-called

*carlos.destefani@uab.es

†xavier.oriols@uab.es

weak values. Since the original single-particle proposal [38], weak values have been attracting a lot of theoretical [39–45] and experimental [46–48] interest in distinct research fields, and a many-particle generalization has been presented by the authors elsewhere [49]. Our goal in this paper is to emphasize that the existence of the *local-in-position weak values* [50] allows novel characterization of quantum systems. One could use distinct types of weak values, but working with weak values of the *momentum* postselected in position allows one to apply all the mathematical machinery (without choosing their ontology) of the Bohmian and stochastic quantum mechanics. For that, in particular, we focus here on how the expectation values of the (squared) real and imaginary parts of such new empirical data allow one to characterize the process of quantum thermalization of a fermionic few-body closed system, defined by a harmonic trap under random disorder. At the end of this paper, we reformulate our proposal in the center-of-mass frame, so that our findings are also extendable to larger systems with many indistinguishable particles.

The paper is organized as follows. Section II presents a brief summary of the needed theoretical background. Section III addresses the orthodox kinetic energy equipartition between its two hidden-variable components. Section IV presents the theoretical model and the numerical results for a particular few-body harmonic trap under random disorder, within three distinct scenarios for the dynamics; the center-of-mass frame is then considered for approaching larger systems. In Sec. V we conclude.

II. THEORETICAL BACKGROUND

This section provides a summary of the needed theoretical background: Sec. II A presents the weak values from the polar form of the many-body wave function, as well as the main equations of both Bohmian quantum mechanics and stochastic quantum mechanics; Sec. II B develops the non-Hermitian expectation values derived from such weak values. Atomic units are employed throughout this paper, which assumes N nonrelativistic spinless particles, each in a one-dimensional (1D) physical space, so that the position in configuration space is $\mathbf{x} = (x_1, \ldots, x_N)$.

A. Weak values postselected in position

A simple path to define the (complex) local-in-position weak value of the momentum for particle j at position $\mathbf{x}$, $p_{W,j}(\mathbf{x}, t)$, linked to the Hermitian operator for the momentum, $\hat{p}_j = -i\,\partial/\partial x_j$, comes after inserting the identity $\int d\mathbf{x}|\mathbf{x}\rangle\langle\mathbf{x}|$ into the expectation value $\langle\Psi(t)|\hat{p}_j|\Psi(t)\rangle$,

$$\langle\hat{p}_j\rangle = \langle\Psi(t)|\hat{p}_j|\Psi(t)\rangle = \int d\mathbf{x}|\Psi(\mathbf{x}, t)|^2\frac{\langle\mathbf{x}|\hat{p}_j|\Psi(t)\rangle}{\langle\mathbf{x}|\Psi(t)\rangle}. \quad (1)$$

From the polar form of the wave function, $\Psi(\mathbf{x}, t) = R(\mathbf{x}, t)\exp(iS(\mathbf{x}, t))$ with $|\Psi(\mathbf{x}, t)|^2 = R^2(\mathbf{x}, t)$, the weak value as stated in (1) decomposes as

$$p_{W,j}(\mathbf{x}, t) \equiv \frac{\langle\mathbf{x}|\hat{p}_j|\Psi(t)\rangle}{\langle\mathbf{x}|\Psi(t)\rangle} = \frac{\partial S(\mathbf{x}, t)}{\partial x_j} - i\frac{1}{R(\mathbf{x}, t)}\frac{\partial R(\mathbf{x}, t)}{\partial x_j}$$
$$= v_j(\mathbf{x}, t) - i\,u_j(\mathbf{x}, t), \quad (2)$$

where the current $v_j(\mathbf{x}, t)$ and osmotic $u_j(\mathbf{x}, t)$ velocities for particle j are identified in (2) as

$$v_j(\mathbf{x}, t) = \frac{\partial S(\mathbf{x}, t)}{\partial x_j} = \mathrm{Im}\left[\frac{1}{\Psi(\mathbf{x}, t)}\frac{\partial\Psi(\mathbf{x}, t)}{\partial x_j}\right], \quad (3)$$

$$u_j(\mathbf{x}, t) = \frac{1}{R(\mathbf{x}, t)}\frac{\partial R(\mathbf{x}, t)}{\partial x_j} = \mathrm{Re}\left[\frac{1}{\Psi(\mathbf{x}, t)}\frac{\partial\Psi(\mathbf{x}, t)}{\partial x_j}\right]. \quad (4)$$

Notice that $v_j(\mathbf{x}, t)$ and $u_j(\mathbf{x}, t)$ depend only on the phase and on the amplitude, respectively, of $\Psi(\mathbf{x}, t)$. The strategy above in fact can be used for any operator; for the bilinear momentum, $\hat{p}_j\hat{p}_l = -\partial/\partial x_j\partial/\partial x_l$, one has

$$\langle\hat{p}_j\hat{p}_l\rangle = \langle\Psi(t)|\hat{p}_j\hat{p}_l|\Psi(t)\rangle = \int d\mathbf{x}|\Psi(\mathbf{x}, t)|^2\frac{\langle\mathbf{x}|\hat{p}_j\hat{p}_l|\Psi(t)\rangle}{\langle\mathbf{x}|\Psi(t)\rangle}, \quad (5)$$

where the bilinear weak value $p_{W,jl}(\mathbf{x}, t)$ is

$$p_{W,jl}(\mathbf{x}, t) \equiv \frac{\langle\mathbf{x}|\hat{p}_j\hat{p}_l|\Psi(t)\rangle}{\langle\mathbf{x}|\Psi(t)\rangle}$$
$$= v_j(\mathbf{x}, t)v_l(\mathbf{x}, t) - u_j(\mathbf{x}, t)u_l(\mathbf{x}, t) - \frac{\partial u_l(\mathbf{x}, t)}{\partial x_j}$$
$$- i\left(u_j(\mathbf{x}, t)v_l(\mathbf{x}, t) + v_j(\mathbf{x}, t)u_l(\mathbf{x}, t) + \frac{\partial v_l(\mathbf{x}, t)}{\partial x_j}\right), \quad (6)$$

which, for $j = l$, defines the weak value of (twice) the kinetic energy for particle j, $K_{W,j}(\mathbf{x}, t)$,

$$2K_{W,j}(\mathbf{x}, t) \equiv \frac{\langle\mathbf{x}|\hat{p}_j^2|\Psi(t)\rangle}{\langle\mathbf{x}|\Psi(t)\rangle}$$
$$= v_j^2(\mathbf{x}, t) - u_j^2(\mathbf{x}, t) - \frac{\partial u_j(\mathbf{x}, t)}{\partial x_j}$$
$$- i\left(2u_j(\mathbf{x}, t)v_j(\mathbf{x}, t) + \frac{\partial v_j(\mathbf{x}, t)}{\partial x_j}\right). \quad (7)$$

Section II B will show that the imaginary part does not contribute for ensemble values of (2), (6), or (7). One could also define from (2) and (6) the (weak) correlation of the momentum postselected in position, $C_{p_{W,j};p_{W,l}} \equiv \langle p_{W,jl}(\mathbf{x}, t)\rangle - \langle p_{W,j}(\mathbf{x}, t)\rangle\langle p_{W,l}(\mathbf{x}, t)\rangle$, as

$$C_{p_{W,j};p_{W,l}} = -\left\langle\frac{\partial u_l(\mathbf{x}, t)}{\partial x_j}\right\rangle - i\left\langle\frac{\partial v_l(\mathbf{x}, t)}{\partial x_j}\right\rangle, \quad (8)$$

which could be used in situations where separated entanglements in phase and amplitude of $\Psi(\mathbf{x}, t)$ were accessible [51], since the real (imaginary) part of $C_{p_{W,j};p_{W,l}}$ depends only on the amplitude (phase) of $\Psi(\mathbf{x}, t)$. Some given properties between current (3) and osmotic (4) velocities will prove important in our derivation. For that, one can use some basic elements of both Bohmian and stochastic quantum mechanics.

1. Bohmian quantum mechanics

The Bohmian theory assumes that particles follow well-defined trajectories guided by $\Psi(\mathbf{x}, t)$, the solution of the Schrödinger equation

$$i\frac{\partial\Psi(\mathbf{x}, t)}{\partial t} = H(\mathbf{x})\Psi(\mathbf{x}, t), \quad (9)$$

whose Hamiltonian is

$$H(\mathbf{x}) = -\frac{1}{2}\sum_{j=1}^{N}\frac{\partial^2}{\partial x_j^2} + V(\mathbf{x}) = K(\mathbf{x}) + V(\mathbf{x}), \quad (10)$$

with $K(\mathbf{x}) = \sum_{j=1}^{N} K_j(x_j)$, where $K_j(x_j) \equiv -\partial^2/2\partial x_j^2$ is the orthodox kinetic energy of each of the N particles, whose interaction is given by the potential energy $V(\mathbf{x})$. From the polar form of $\Psi(\mathbf{x}, t)$, Eq. (9) gets rewritten as two coupled equations. On the one hand, the imaginary part yields the continuity equation,

$$\frac{\partial R^2(\mathbf{x}, t)}{\partial t} + \sum_{j=1}^{N}\frac{\partial}{\partial x_j}\left(R^2(\mathbf{x}, t)\frac{\partial S(\mathbf{x}, t)}{\partial x_j}\right) = 0, \quad (11)$$

in which from (3) one identifies the j component of the current density as $J_j(\mathbf{x}, t) \equiv R^2(\mathbf{x}, t)v_j(\mathbf{x}, t)$. On the other hand, the real part yields the quantum Hamilton-Jacobi equation,

$$\frac{\partial S(\mathbf{x}, t)}{\partial t} + K_B(\mathbf{x}, t) + Q_B(\mathbf{x}, t) + V(\mathbf{x}) = 0, \quad (12)$$

with $K_B(\mathbf{x}, t) = \sum_{j=1}^{N} K_{B,j}(\mathbf{x}, t)$ and $Q_B(\mathbf{x}, t) = \sum_{j=1}^{N} Q_{B,j}(\mathbf{x}, t)$, where the j components of the Bohmian kinetic $K_{B,j}(\mathbf{x}, t)$ and quantum potential $Q_{B,j}(\mathbf{x}, t)$ energies are

$$K_{B,j}(\mathbf{x}, t) = \frac{1}{2}\left(\frac{\partial S(\mathbf{x}, t)}{\partial x_j}\right)^2, \quad (13)$$

$$Q_{B,j}(\mathbf{x}, t) = -\frac{1}{2R(\mathbf{x}, t)}\frac{\partial^2 R(\mathbf{x}, t)}{\partial x_j^2}. \quad (14)$$

The Bohmian trajectories, thanks to the current density $J_j(\mathbf{x}, t)$ in (11), are obtained from the integration solely of $v_j(\mathbf{x}, t)$ [$u_j(\mathbf{x}, t)$ plays no role]; so, throughout this paper, $v_j(\mathbf{x}, t)$ is interchangeably identified either as the Bohmian velocity or the current velocity. In Bohmian theory, while the kinetic energy is determined by the phase of the wave function, the quantum potential, determined by its amplitude, has indeed the status of a potential energy since, from a time derivative in (3) and by using (12), one gets the set of Newton-like equations,

$$\frac{d^2 x_j(t)}{dt^2} = -\left[\frac{\partial}{\partial x_j}(V(\mathbf{x}, t) + Q_B(\mathbf{x}, t))\right]_{\mathbf{x}=\mathbf{x}(t)}, \quad (15)$$

which is another way of getting the Bohmian trajectories.

2. Stochastic quantum mechanics

The stochastic quantum mechanics may be understood as an attempt to give a kinematic interpretation also to the quantum potential, although such a potential is not explicit in its original derivation. Notice indeed that, from (3) and (4), Eqs. (13) and (14) can be cast into

$$K_{B,j}(\mathbf{x}, t) = \frac{1}{2}v_j^2(\mathbf{x}, t), \quad (16)$$

$$Q_{B,j}(\mathbf{x}, t) = -\frac{1}{2}u_j^2(\mathbf{x}, t) - \frac{1}{2}\frac{\partial u_j(\mathbf{x}, t)}{\partial x_j}, \quad (17)$$

so that $K_{B,j}(\mathbf{x}, t)$ and $Q_{B,j}(\mathbf{x}, t)$ depend only on Bohmian and osmotic velocities, respectively. Notice that $K_{B,j}(\mathbf{x}, t)$ and

$Q_{B,j}(\mathbf{x}, t)$ are not weak values computed from the Hermitian operator of the kinetic energy, as happens with $K_{W,j}(\mathbf{x}, t)$ in (7). One should keep in mind that according to this stochastic theory, $v_j(\mathbf{x}, t) + u_j(\mathbf{x}, t)$ has the meaning of a mean velocity, while the true velocity is a random velocity around it. Such a theory is defined in terms of a stochastic diffusion process in the configuration space, which requires that the probability $R^2(\mathbf{x}, t)$ satisfies both forward (+) and backward (−) Fokker-Planck equations for a parameter ν,

$$\frac{\partial R^2(\mathbf{x}, t)}{\partial t} = -\sum_j \frac{\partial}{\partial x_j}((v_j(\mathbf{x}, t) \pm u_j(\mathbf{x}, t))R^2(\mathbf{x}, t))$$
$$\pm \nu \sum_j \frac{\partial^2 R^2(\mathbf{x}, t)}{\partial x_j^2}, \quad (18)$$

whose sum yields the continuity equation in (11), irrespective of $u_j(\mathbf{x}, t)$ and ν, and whose difference yields

$$\nu \frac{\partial^2 R^2(\mathbf{x}, t)}{\partial x_j^2} = \frac{\partial(u_j(\mathbf{x}, t)R^2(\mathbf{x}, t))}{\partial x_j}, \quad (19)$$

which is satisfied by the $u_j(\mathbf{x}, t)$ in (4) and with $\nu = 1/2$. In other words, the Fokker-Planck equations in (18), with (4) and $\nu = 1/2$, delineate a picture using (19) in which the osmotic current $u_j(\mathbf{x}, t)R^2(\mathbf{x}, t)$ is balanced by some diffusion current $\nu\partial R^2(\mathbf{x}, t)/\partial x_j$, so that the continuity equation in (11) remains valid and determined solely by the current velocity $v_j(\mathbf{x}, t)$. As such, the kinematic interpretation of the quantum potential, implicit in the derivation of the stochastic quantum mechanics, empirically reproduces both Bohmian and orthodox quantum mechanics.

B. Expectation values from weak values

From (1) and (2) the expectation value for the momentum weak value postselected in position, $\langle p_{W,j} \rangle$, is

$$\langle \hat{p}_j \rangle = \int d\mathbf{x}\, p_{W,j}(\mathbf{x}, t)|\Psi(\mathbf{x}, t)|^2 \equiv \langle p_{W,j} \rangle. \quad (20)$$

For this particular case one can directly compute the expectation values of each of its real and imaginary parts, yielding from (1) and (2)

$$\langle v_j \rangle = \int d\mathbf{x}\, \text{Re}[p_{W,j}(\mathbf{x}, t)]|\Psi(\mathbf{x}, t)|^2 = \langle \hat{p}_j \rangle, \quad (21)$$

$$\langle u_j \rangle = \int d\mathbf{x}\, \text{Im}[p_{W,j}(\mathbf{x}, t)]|\Psi(\mathbf{x}, t)|^2 = 0, \quad (22)$$

so that, while $v_j(\mathbf{x}, t) \neq p_{W,j}(\mathbf{x}, t)$, $\langle v_j \rangle = \langle p_{W,j} \rangle$ and the osmotic velocity has no role in the expectation values of either $\hat{p}_j$ or $p_{W,j}(\mathbf{x}, t)$ (for a wave function vanishing at the system borders). Strictly speaking, $v_j(\mathbf{x}, t)$ and $u_j(\mathbf{x}, t)$ are not weak values themselves, but they are postprocessed real and imaginary parts, respectively, of the weak value $p_{W,j}(\mathbf{x}, t)$. In other words, while $p_{W,j}(\mathbf{x}, t)$ is linked to the Hermitian operator $\hat{p}_j$, no Hermitian operators can be linked to $v_j(\mathbf{x}, t)$ or $u_j(\mathbf{x}, t)$. The connection between $p_{W,j}(\mathbf{x}, t)$ and $v_j(\mathbf{x}, t)$ is approached elsewhere [52–59], while more attention has recently been paid to the meaning of $u_j(\mathbf{x}, t)$ [60–68]. We distinguish in this paper three types of expectation values: (i) $\langle \hat{a} \rangle$, with the "hat," for the operator $\hat{a}$; (ii) $\langle a_W \rangle$, with subscript "W," for

the weak value a_W; and (iii) $\langle a \rangle$ for the value a obtained by postprocessing the weak value.

The expectation value of the bilinear weak value, $\langle p_{W,jl} \rangle$, is from (5) and (6)

$$
\begin{aligned}
\langle \hat{p}_j \hat{p}_l \rangle &= \int d\mathbf{x} \, p_{W,jl}(\mathbf{x},t) |\Psi(\mathbf{x},t)|^2 \\
&= \langle v_j v_l \rangle + \langle u_j u_l \rangle \equiv \langle p_{W,jl} \rangle,
\end{aligned}
\tag{23}
$$

where we have used

$$
\left\langle \frac{\partial u_l}{\partial x_j} \right\rangle = -2 \langle u_l u_j \rangle,
\tag{24}
$$

$$
\left\langle \frac{\partial v_l}{\partial x_j} \right\rangle = -\langle u_l v_j \rangle - \langle v_l u_j \rangle;
\tag{25}
$$

for an antisymmetric $\Psi(\mathbf{x},t)$, one has $\langle u_l v_j \rangle = \langle v_l u_j \rangle$. Once more, the weak value $p_{W,jl}(\mathbf{x},t)$ is linked to $\hat{p}_j \hat{p}_l$, but $v_j(\mathbf{x},t) v_l(\mathbf{x},t)$ and $u_j(\mathbf{x},t) u_l(\mathbf{x},t)$ are just postprocessed data obtained from the real and imaginary parts of the weak values $p_{W,j}(\mathbf{x},t)$ and $p_{W,l}(\mathbf{x},t)$. Interestingly, from (24) the expectation values of the Bohmian kinetic $\langle K_{B,j} \rangle$ and quantum potential $\langle Q_{B,j} \rangle$ energies in (16) and (17) become

$$
\langle K_{B,j} \rangle = \tfrac{1}{2} \langle v_j^2 \rangle,
\tag{26}
$$

$$
\langle Q_{B,j} \rangle = \tfrac{1}{2} \langle u_j^2 \rangle,
\tag{27}
$$

$$
\langle \hat{K}_j \rangle = \tfrac{1}{2} \left(\langle v_j^2 \rangle + \langle u_j^2 \rangle \right),
\tag{28}
$$

where the last equation is the expectation value of the orthodox kinetic energy, $\langle \hat{K}_j \rangle = \langle \hat{p}_j^2 \rangle / 2$, as promptly obtained from (23). Neither $\langle v_j^2 \rangle$ nor $\langle u_j^2 \rangle$ are expectation values of a weak value; they are instead expectation values of the (squared) real and imaginary parts, respectively, of the weak value $p_{W,j}(\mathbf{x},t)$. Notice that by integrating the weak values of the kinetic energy in (7) with the use of (24) and (25) and comparing the result with (28), one obtains

$$
\langle \hat{K}_j \rangle = \int d\mathbf{x} \, K_{W,j}(\mathbf{x},t) |\Psi(\mathbf{x},t)|^2 = \langle K_{W,j} \rangle.
\tag{29}
$$

Similar to the (weak) correlation in (8), one can define the correlations $C_{\hat{a},\hat{b}} \equiv \langle \hat{a}\hat{b} \rangle - \langle \hat{a} \rangle \langle \hat{b} \rangle$ between operators and $C_{a,b} \equiv \langle ab \rangle - \langle a \rangle \langle b \rangle$ between quantities postprocessed from weak values. For the momentum operator, from (23) and (21) one obtains

$$
C_{\hat{p}_j, \hat{p}_l} = \langle v_j v_l \rangle + \langle u_j u_l \rangle - \langle v_j \rangle \langle v_l \rangle = C_{v_j, v_l} + C_{u_j, u_l},
\tag{30}
$$

$$
C_{p_{W,j}; p_{W,l}} = 2 \langle u_j u_l \rangle + i(\langle u_j v_l \rangle + \langle v_j u_l \rangle),
\tag{31}
$$

where (22) is used in (30), while (31) results from applying (24) and (25) in (8). So, while the Bohmian velocity fully determines $\langle \hat{p}_j \rangle$ in (21), the osmotic velocity, although satisfying (22), induces a deviation between the quantum correlations of the momentum with respect to the current velocity in (30). Notice that from (30) and (31) one has $\mathrm{Re}[C_{p_{W,j}; p_{W,l}}] = 2C_{u_j, u_l}$, while one should have $\mathrm{Im}[C_{p_{W,j}; p_{W,l}}] \approx 0$.

III. EQUIPARTITION AT THERMALIZATION OF THE HIDDEN-VARIABLE COMPONENTS

Since the expectation values $\langle K_{B,j} \rangle$ and $\langle Q_{B,j} \rangle$ cannot be computed from Hermitian operators, the typical argumentation of ETH to discuss thermalization of observables cannot directly be applied to these quantities, although the very same spirit can still be used. For that, let us first summarize the usual interpretation of the thermalization of expectation values.

From an initial nonequilibrium state $|\Psi(0)\rangle$, whose unitary evolution is dictated by $|\Psi(t)\rangle = \sum_n c_n e^{-i\omega_n t} |n\rangle$, with $|n\rangle$ being an energy eigenstate with eigenvalue ω_n and with $c_n = \langle n|\Psi(0)\rangle$ being defined by initial conditions, the expectation value of some Hermitian operator $\hat{a}$ reads

$$
\langle \hat{a} \rangle = \sum_n \rho_{n,n}(0) a_{n,n} + \sum_{n,m \neq n} \rho_{n,m}(t) a_{m,n},
\tag{32}
$$

with $a_{m,n} = \langle m|\hat{a}|n\rangle$ and with $\rho_{n,m}(t) = c_m^* c_n e^{i(\omega_m - \omega_n)t}$ being the density matrix, composed of diagonal time-independent and nondiagonal time-dependent terms; while the former can never be neglected (unless it is zero by construction), the latter needs to be negligible after some given time if one expects $\langle \hat{a} \rangle$ to thermalize. A system is said to equilibrate if, after some time t_{eq} long enough for full dephasing between different energy eigenstates, the nondiagonal terms cancel out so that (32) can solely be computed from the diagonal terms, $\langle \hat{a} \rangle \approx \sum_n \rho_{n,n}(0) a_{n,n}$, for most times $t > t_{eq}$. The system is then said to thermalize when $\langle \hat{a} \rangle$ becomes roughly equal to the expectation value as computed from its microcanonical density matrix. The ETH states that such dephasing is more typical in nondegenerate and chaotic many-body scenarios, where the nondiagonals $a_{m,n}$ in (32) become exponentially smaller than the diagonals $a_{n,n}$. In other words, a nonequilibrium state whose evolution involves a large number of eigenstates (not necessarily of particles) is required [69]. Such a picture immediately applies to the thermalization of the orthodox kinetic $K(\mathbf{x})$ and potential $V(\mathbf{x})$ operators in (10). For the hidden-variable components of the Bohmian and stochastic kinetic energies, however, one needs an extra step, which renders us the main result of our work in what follows.

The Bohmian velocity for particle j is, from (3),

$$
v_j(\mathbf{x},t) = \mathrm{Im}\left[\frac{1}{\Psi(\mathbf{x},t)} \frac{\partial \Psi(\mathbf{x},t)}{\partial x_j} \right] = \frac{1}{2i}\left(\frac{\tilde{\Psi}_j}{\Psi} - \frac{\tilde{\Psi}_j^*}{\Psi^*} \right),
\tag{33}
$$

where $\tilde{\Psi}_j \equiv \partial \Psi(\mathbf{x},t) / \partial x_j$ and $\Psi \equiv \Psi(\mathbf{x},t)$. The ensemble value of the product $\langle v_j v_l \rangle$ is

$$
\begin{aligned}
\langle v_j v_l \rangle &= \int d\mathbf{x} |\Psi(\mathbf{x},t)|^2 \, v_j(\mathbf{x},t) v_l(\mathbf{x},t) \\
&= -\frac{1}{4} \int d\mathbf{x} \frac{1}{|\Psi|^2} (\tilde{\Psi}_j \Psi^* - \tilde{\Psi}_j^* \Psi)(\tilde{\Psi}_l \Psi^* - \tilde{\Psi}_l^* \Psi) \\
&= \frac{1}{2} \int d\mathbf{x} \, \tilde{\Psi}_j \tilde{\Psi}_l^* \\
&\quad - \frac{1}{4} \int d\mathbf{x} \frac{1}{|\Psi|^2} (\tilde{\Psi}_j \Psi^* \tilde{\Psi}_l \Psi^* + \tilde{\Psi}_j^* \Psi \tilde{\Psi}_l^* \Psi).
\end{aligned}
\tag{34}
$$

The first integral is just half of $\langle \hat{p}_j \hat{p}_l \rangle = \langle (\hat{p}_j \Psi(t))^*|\hat{p}_l \Psi(t) \rangle = \int d\mathbf{x} \, \tilde{\Psi}_j \tilde{\Psi}_l^*$, which then follows

the same thermalization process discussed after (32) for Hermitian operators. The second integral is the sum of one component plus its complex conjugate so that (34) remains indeed real. As discussed in the Appendix, this second integral yields a sum of random numbers around zero with vanishing contribution, so that the thermalized value of (34) becomes

$$\langle v_j v_l \rangle \approx \frac{\langle \hat{p}_j \hat{p}_l \rangle}{2}. \tag{35}$$

From exactly the same procedure, since the osmotic velocity for particle j is, from (4),

$$u_j(\mathbf{x}, t) = \mathrm{Re}\left[\frac{1}{\Psi(\mathbf{x}, t)} \frac{\partial \Psi(\mathbf{x}, t)}{\partial x_j} \right] = \frac{1}{2}\left(\frac{\tilde{\Psi}_j}{\Psi} + \frac{\tilde{\Psi}_j^*}{\Psi^*} \right), \tag{36}$$

the ensemble value of the product $\langle u_j u_l \rangle$ will be exactly the same as in (34), but with a positive sign in the second integral. Thus, applying the same reasoning as above, one finds the thermalized value

$$\langle u_j u_l \rangle \approx \frac{\langle \hat{p}_j \hat{p}_l \rangle}{2}, \tag{37}$$

so that (23) remains satisfied after thermalization.

Applying (35) and (37) with $j = l$ into (26)–(28) yields

$$\langle \hat{K}_j \rangle = \langle K_{B,j} \rangle + \langle Q_{B,j} \rangle, \tag{38}$$

$$\frac{\langle \hat{K}_j \rangle}{2} \approx \langle K_{B,j} \rangle \approx \langle Q_{B,j} \rangle. \tag{39}$$

While (38) is already true in (26)–(28), and so is valid in any scenario, thermalized or not, the *kinetic energy equipartition* in (39), being only valid at times $t > t_{eq}$, presents the *hidden-variable signature* of quantum thermalization: Bohmian kinetic and quantum potential energies become equal, with each being equal to half of the orthodox kinetic energy. Similarly, while $\langle \hat{p}_j^2 \rangle = \langle v_j^2 \rangle + \langle u_j^2 \rangle$ applies at any time, at $t > t_{eq}$, $\langle \hat{p}_j^2 \rangle / 2 \approx \langle v_j^2 \rangle \approx \langle u_j^2 \rangle$ should also apply. That is, thermalization also implies that (squared) Bohmian and osmotic velocities become equal, with each being equal to half of the (squared) orthodox momentum; in other words, information from the phase of the wave function and information from the amplitude of the wave function become similar after $t > t_{eq}$, which is a result of the initially localized wave function, in a nonequilibrium dynamics, spreading almost homogeneously through the whole configuration space after the onset of thermalization. In addition to (38) and (39), and particularly for a randomly disordered harmonic trap, one should also find

$$\langle \hat{H} \rangle = \langle \hat{K} \rangle + \langle \hat{V} \rangle, \tag{40}$$

$$\frac{\langle \hat{H} \rangle}{2} \approx \langle \hat{K} \rangle \approx \langle \hat{V} \rangle. \tag{41}$$

Equation (40) expresses the conservation of total energy, from the Hamiltonian in (10) in a unitary evolution, valid at any time. Equation (41) tells us that the orthodox virial theorem, as one reaches some steady state at $t > t_{eq}$, is expected to be restated; that is, potential and kinetic energies should become

equal, with each being equal to half of the total energy. It is assumed in (40) and (41) that $\langle \hat{V} \rangle$ mostly comes from the confining potential. At last, from entering (35) and (37) into (30) and (31), the thermalized correlations should satisfy

$$\frac{C_{\hat{p}_j, \hat{p}_l}}{2} \approx C_{v_j, v_l} \approx C_{u_j, u_l} \approx \frac{C_{p_{w,j}; p_{w,l}}}{2}. \tag{42}$$

IV. NUMERICAL RESULTS

The nonequilibrium initial state and the Hamiltonian of our model are found in Sec. IV A, Sec. IV B addresses our results according to three scenarios with distinct initial conditions, and in Sec. IV C we reformulate our model in the center-of-mass frame.

A. Initial state and trap Hamiltonian

The initial N-electron nonequilibrium pure antisymmetric state is

$$\langle \mathbf{x} | \Psi(0) \rangle = \frac{1}{\mathcal{C}} \sum_{n=1}^{N!} \mathrm{sgn}(\vec{p}(n)) \prod_{j=1}^{N} \psi_j(x_{p(n)_j}, 0), \tag{43}$$

with $\mathcal{C}$ being a normalization constant and $\mathrm{sgn}(\vec{p}(n))$ being the sign of the permutation $\vec{p}(n) = \{p(n)_1, \ldots, p(n)_N\}$. Each initial Gaussian state in (43) is

$$\psi_j(x, 0) = \exp\left[-\frac{(x - x_{0j})^2}{2\sigma_j^2} \right] \exp[i p_{0j}(x - x_{0j})], \tag{44}$$

with spatial dispersion σ_j, central position x_{0j}, and central velocity p_{0j}. Any nonzero x_{0j} or p_{0j} may activate the nonequilibrium dynamics.

The Hamiltonian $H(\mathbf{x})$ propagating the many-body wave function $\Psi(\mathbf{x}, t)$ is given in (10), where the kinetic term $K(\mathbf{x})$ is already defined. The potential term $V(\mathbf{x})$, in our disordered harmonic trap, is defined by

$$V(\mathbf{x}) \equiv V_H(\mathbf{x}) + V_I(\mathbf{x}) + V_D(\mathbf{x}), \tag{45}$$

where the harmonic potential $V_H(\mathbf{x})$ with frequency ω is

$$V_H(\mathbf{x}) = \frac{1}{2}\omega^2 \sum_{j=1}^{N} x_j^2 \tag{46}$$

and the electron-electron interaction potential $V_I(\mathbf{x})$ with smooth parameter α is

$$V_I(\mathbf{x}) = \frac{1}{2} \sum_{j=1}^{N} \sum_{l \neq j}^{N} \frac{1}{\sqrt{(x_j - x_l)^2 + \alpha^2}}. \tag{47}$$

To ensure that the initial state in (43) is built as a superposition of a large (and "chaotic") number of eigenstates, we include the random disorder potential $V_D(\mathbf{x})$,

$$V_D(\mathbf{x}) = \gamma_D \sum_{j=1}^{N} \sum_{l=1}^{M} b_l \exp\left[-\frac{4(x_j - g_l)^2}{\sigma_D^2} \right], \tag{48}$$

where γ_D is its strength and σ_D is its spatial dispersion, with g_l running through M grid points; the set of random numbers b_l satisfies $\langle b_l \rangle = 0$ and $\langle b_l^2 \rangle = 1$, and the disorder potential is normalized so that the integral of $V_D^2(\mathbf{x})$ yields γ_D^2. Such

TABLE I. The three scenarios, D1, D2, and D3, for the dynamics with and without disorder for $N = 2$. The first two rows show values of (x_{01}, x_{02}) and (p_{01}, p_{02}) for the initial nonequilibrium state. The last three rows show features of the expectation values of $(\langle x \rangle, \langle p \rangle)$ and of orthodox $(\langle K \rangle, \langle V_H \rangle)$ and Bohmian $(\langle K_B \rangle, \langle Q_B \rangle)$ energies. The symbol $\checkmark$ ($\times$) indicates that such expectation values allow (do not allow) one to identify t_{eq}.

	Scenario D1		Scenario D2		Scenario D3	
Disorder	No	Yes	No	Yes	No	Yes
(x_{01}, x_{02})	$(-2, 2)$	$(-20, 20)$	$(-2, 2)$	$(-2, 2)$	$(-2, 2)$	$(-20, 20)$
(p_{01}, p_{02})	$(0,0)$	$(0,0)$	$(4,4)$	$(20,20)$	$(2,2)$	$(20,20)$
$(\langle x \rangle, \langle p \rangle)$		$\times$		$\checkmark$		$\checkmark$
$(\langle K \rangle, \langle V_H \rangle)$		$\checkmark$		$\checkmark$		$\times$
$(\langle K_B \rangle, \langle Q_B \rangle)$		$\checkmark$		$\checkmark$		$\checkmark$

a shape is typical of speckle potentials [70–76] in fermionic traps.

B. Expectation values in three scenarios

Our results initially focus on $N = 2$. However, our main conclusions, as the kinetic energy equipartition at thermalization, are valid for any N as the discussion in the center-of-mass frame will later settle. We focus on three scenarios, D1, D2, and D3, which are distinct in terms of the initial values of x_{0j} and p_{0j}, as summarized in Table I, where each scenario considers both dynamics with no disorder and dynamics with disorder. Values of x_{0j} in scenario D1 and p_{0j} in scenario D2 are chosen to be identical so as to yield the same turning points in both dynamics; the remaining simulation parameters are found in Ref. [77]. The no-disorder cases employ smaller values of x_{0j} and p_{0j} to render the features more visible.

The dynamics for scenarios D1, D2, and D3 is shown in Figs. 1–3, respectively: Panels (a)–(d) in each figure show a few initial cycles with no disorder, and panels (e)–(h) show the full evolution with disorder. The structure of these three figures, which focus on the time evolution of some pertinent expectation values, is as follows: Panels (a) and (e) show kinetic $\langle K \rangle$, harmonic $\langle V_H \rangle$, interaction $\langle V_I \rangle$, and total $\langle H \rangle = \langle K \rangle + \langle V_H \rangle + \langle V_I \rangle + \langle V_D \rangle$ energies, with disorder energy $\langle V_D \rangle \approx 0$ at any t not shown; panels (b) and (f) show Bohmian velocity $\langle v_j \rangle$, position $\langle x_j \rangle$, and osmotic velocity $\langle u_j \rangle$, with momentum $\langle p_j \rangle = \langle v_j \rangle$ not shown, and the label j is not indicated since it is redundant in our antisymmetrized model; panels (c) and (g) repeat the orthodox kinetic energy $\langle K \rangle$, for its comparison with the Bohmian kinetic $\langle K_B \rangle$ and quantum potential $\langle Q_B \rangle$ energies; and panels (d) and (h) show the correlations for momentum $C_{\hat{p}_1, \hat{p}_2}$, Bohmian C_{v_1, v_2} and osmotic C_{u_1, u_2} velocities, and position $C_{\hat{x}_1, \hat{x}_2}$.

1. Dynamics from the initial position

Let us first focus on the D1 dynamics without disorder in Figs. 1(a)–1(d), which has $p_{01} = p_{02} = 0$ and a small $x_{01} = -x_{02} = -2$. At $t = 0$, Fig. 1(a) yields $\langle V_H \rangle(0) = x_{01}^2/2 + x_{02}^2/2 + E_V/2 = 4.5$ and $\langle K \rangle(0) = p_{01}^2/2 + p_{02}^2/2 + E_V/2 = 0.5$, where $E_V = \omega(n + 1)$ is the ground state energy ($\omega = 1$, $n = 0$) which is equally shared between potential and kinetic

terms. That is, the virial theorem in (41) is not satisfied (at any t) thanks to the nonequilibrium initial situation; however, the total energy in (40), $\langle H \rangle(0) = 5.27$ since $\langle V_I \rangle(0) = 0.27$, is conserved (at any t) thanks to the unitary evolution. In Fig. 1(c), at $t = 0$, one has $\langle Q_B \rangle(0) = 0.5$ and $\langle K_B \rangle(0) = 0$ [since the initial velocities are zero; see Fig. 1(b)], so that indeed $\langle K \rangle(0) = 0.5$ and (38) is satisfied (at any t), while (39) does not apply here. Each D1 cycle has a π period and three stages. For the first cycle, the following occurs: (i) At $t = 0$, electrons are at $(x_1, x_2) = (-2, 2)$, with minimum $\langle K \rangle$ and maximum $\langle V_H \rangle$; (ii) the dynamics pushes the electrons against each other until, at $t = \pi/2$, they try binding together at $(x_1, x_2) = (0, 0)$, which is avoided thanks to exchange symmetry, Coulomb repulsion, and quantum potential, as indicated by the peak in $\langle V_I \rangle$ and in $\langle Q_B \rangle$, with maximum $\langle K \rangle$ and minimum $\langle V_H \rangle$ and $\langle K_B \rangle$; and (iii) at $t = \pi$, electrons are back to $(x_1, x_2) = (-2, 2)$, and a new cycle starts. Notice that $\langle K_B \rangle$ has a double peak around the peak of $\langle Q_B \rangle$ because the velocity acquires a first maximum from $t = 0$ to $t = \pi/2$, which is the time electrons "stop" to reverse their movements, and a second maximum from $t = \pi/2$ to $t = \pi$. One sees how the quantum potential, acting "in phase" with the Coulomb repulsion, carries the quantumness of the two-body entanglement. The correlations in Fig. 1(d) are a mirror of the above discussion; they are all negative since as one variable increases, the other decreases in the D1 dynamics. In terms of moduli, at $t = 0$, $C_{\hat{x}1, \hat{x}2}$ is at its maximum due to the maximum electron separation, and reaches its vanishing minimum at $t = \pi/2$ when electrons are closest to each other. The three kinetic correlations are zero at $t = 0$ thanks to the same initial zero velocity for the electrons; at $t = \pi/2$, since at that time it is only $\langle Q_B \rangle$ that contributes to $\langle K \rangle$, $C_{u1, u2}$ reaches its maximum while $C_{v1, v2}$ vanishes. Notice that (30) is satisfied at any t, while (42) does not apply here. In Fig. 1(b), $\langle v \rangle = \langle x \rangle = \langle u \rangle = 0$ at any t is a trivial consequence of the D1 dynamics being antidiagonal in the configuration space $x_1 x_2$, with electrons initially equidistant, what anticipates that such terms reflect center-of-mass properties.

The full D1 dynamics with disorder is shown in Figs. 1(e)–1(h). Thanks to the larger $x_{01} = -x_{02} = -20$, the oscillation amplitudes are larger but with the same π period. The magnitude of $\langle V_I \rangle$, though, remains similar to the no-disorder case, such that we magnify it by 100 here, while the initial peaks in $\langle V_I \rangle$ and in $\langle Q_B \rangle$ as well as the minima in $\langle K_B \rangle$ become steeper in the disordered scenario. As the cycles succeed, all expectation values overall reach quasistationary magnitudes once thermalization is set at $t_{eq} \approx 55$. In Fig. 1(e), while maintaining $\langle H \rangle$ constant as in (40), kinetic and potential energies interchange their magnitudes until (41) becomes valid, and the virial theorem appears to be restated after thermalization, seemingly an indication that a thermalized state is reached; the Coulomb repulsion $\langle V_I \rangle$ smears out, and its peaks disappear after thermalization. In Fig. 1(g), while (38) remains true at any t, the peaks in $\langle Q_B \rangle$ and minima in $\langle K_B \rangle$ also smear out and disappear after thermalization. Most interestingly, this happens in such a way as to satisfy (39), allowing one to visualize the central result of this paper: In addition to the "restatement" of the virial theorem, thermalization also implies a kinetic energy equipartition, the hidden-variable signature of quantum thermalization. The trivial values of $\langle x \rangle = \langle v \rangle = \langle u \rangle \approx 0$
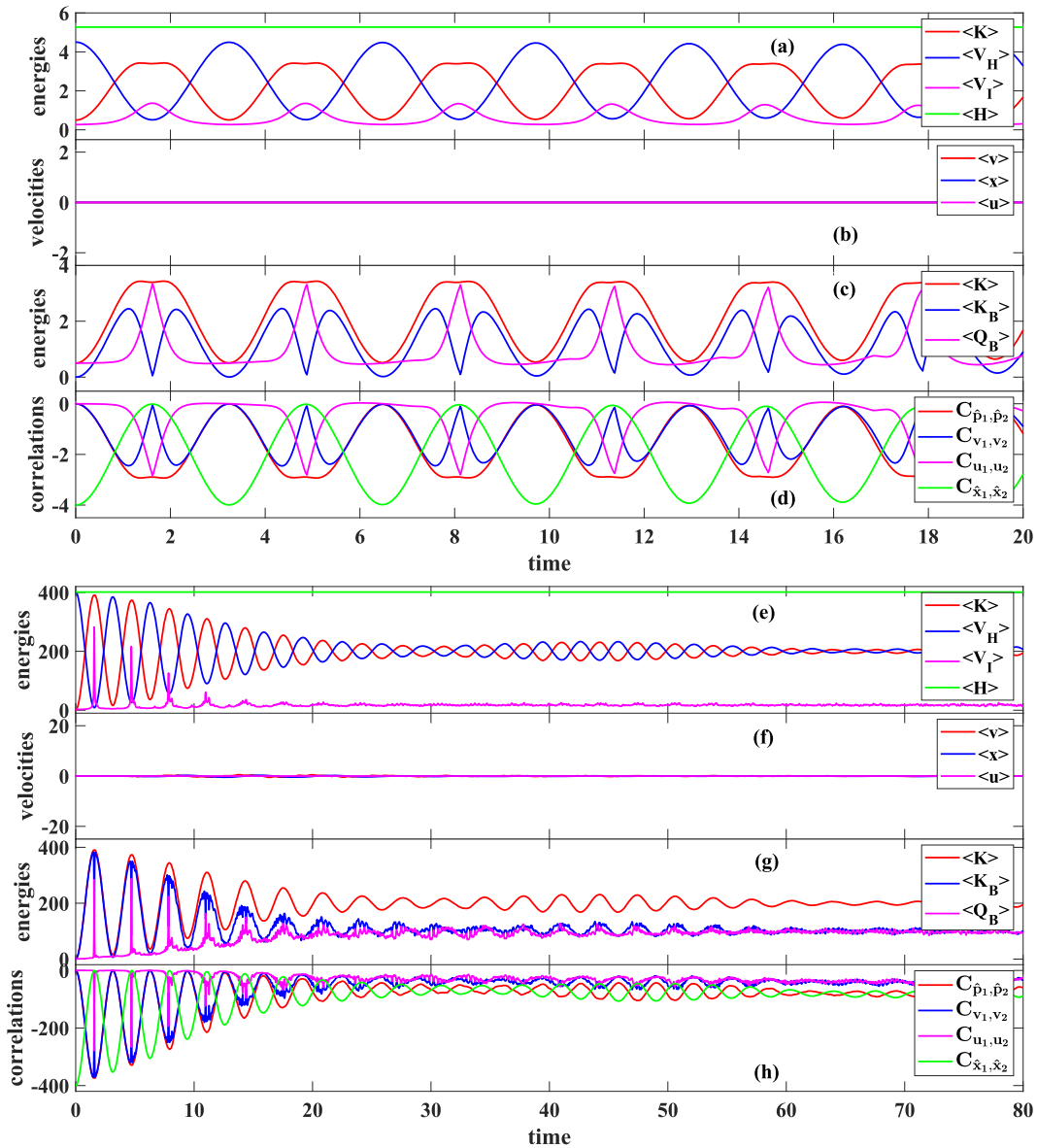
FIG. 1. Expectation values from the dynamics in scenario D1, with $(p_{01}, p_{02}) = (0, 0)$. (a)–(d) A few initial cycles under no disorder with a smaller $(x_{01}, x_{02}) = (-2, 2)$; (e)–(h) full dynamics under disorder with a larger $(x_{01}, x_{02}) = (-20, 20)$. (a) and (e) show energies: orthodox kinetic energy $\langle K \rangle$, harmonic confining energy $\langle V_H \rangle$, Coulomb repulsion energy $\langle V_I \rangle$, and total energy $\langle H \rangle$ [$\langle V_I \rangle$ is magnified by 100 in (e)]. (b) and (f) show velocities: Bohmian velocity $\langle v \rangle$, position $\langle x \rangle$, and osmotic velocity $\langle u \rangle$. (c) and (g) show a comparison of the kinetic energies: orthodox $\langle K \rangle$, Bohmian $\langle K_B \rangle$, and quantum potential $\langle Q_B \rangle$ energies. (d) and (h) show correlations: momentum $C_{\hat{p}_1, \hat{p}_2}$, Bohmian C_{v_1, v_2} and osmotic C_{u_1, u_2} velocities, and position $C_{\hat{x}_1, \hat{x}_2}$. All quantities in atomic units.

remain at any t in Fig. 1(f) and so present no feature to identify thermalization. The correlations in Fig. 1(h) are once more a mirror of the above discussion, so the maxima and minima of the initial cycles smear out after thermalization, when one also finds that, in addition to (30), Eq. (42) is also satisfied, as well as $C_{\hat{p}_1, \hat{p}_2} \approx C_{\hat{x}_1, \hat{x}_2}$; the correlations remain negative, reaching small values after t_{eq}.

2. Dynamics from the initial velocity

Let us start the discussion of the D2 dynamics once more from the no-disorder case in Figs. 2(a)–2(d), which has $x_{01} = -x_{02} = -2$ [as $(x_{01}, x_{02}) = (0, 0)$ cannot be used in a

fermionic trap] and a small $p_{01} = p_{02} = 4$ (such that both electrons start moving in the same direction). As such, at $t = 0$, one still has $\langle V_H \rangle(0) = 4.5$ and $\langle V_I \rangle(0) = 0.27$, but a larger $\langle K \rangle(0) = 16.5$, built from $\langle K_B \rangle(0) = 16$ and $\langle Q_B \rangle(0) = 0.5$, so yielding $\langle H \rangle(0) = 21.27$. Each D2 cycle has a 2π period and five stages. The first cycle is as follows: (i) At $t = 0$, electrons are at $(x_1, x_2) = (-2, 2)$ with minimum $\langle V_H \rangle$ and maximum $\langle K \rangle$; (ii) at $t = \pi/2$, electrons reach the positive turning point and try to collide at $(x_1, x_2) = (4, 4)$, yielding peaks in $\langle V_I \rangle$ and in $\langle Q_B \rangle$, while $\langle K_B \rangle = 0$ as the electrons stop at that time (the fact that the peak in $\langle Q_B \rangle$ is now at the minimum of $\langle K \rangle$ is the reason why a double peak is no longer seen in $\langle K_B \rangle$ contrarily to the D1 scenario); (iii) at $t = \pi$,
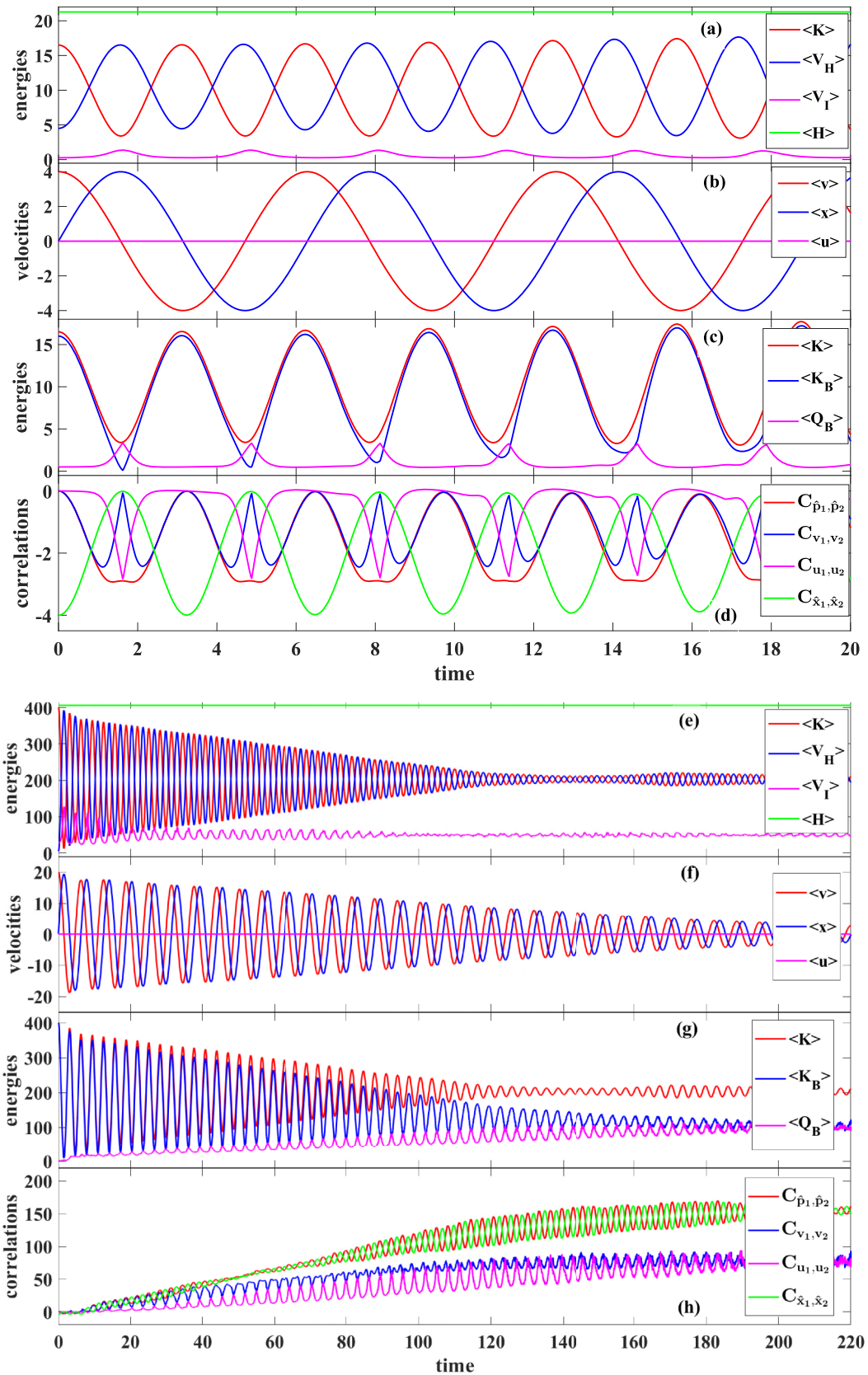
FIG. 2. Expectation values from the dynamics in scenario D2, with $(x_{01}, x_{02}) = (-2, 2)$. (a)–(d) A few initial cycles under no disorder with a smaller $(p_{01}, p_{02}) = (4, 4)$; (e)–(h) full dynamics under disorder with a larger $(p_{01}, p_{02}) = (20, 20)$. (a) and (e) show energies: orthodox kinetic energy $\langle K \rangle$, harmonic confining energy $\langle V_H \rangle$, Coulomb repulsion energy $\langle V_I \rangle$, and total energy $\langle H \rangle$ [$\langle V_I \rangle$ is magnified by 100 in (e)]. (b) and (f) show velocities: Bohmian velocity $\langle v \rangle$, position $\langle x \rangle$, and osmotic velocity $\langle u \rangle$. (c) and (g) show a comparison of the kinetic energies: orthodox $\langle K \rangle$, Bohmian $\langle K_B \rangle$, and quantum potential $\langle Q_B \rangle$ energies. (d) and (h) show correlations: momentum $C_{\hat{p}_1, \hat{p}_2}$, Bohmian C_{v_1, v_2} and osmotic C_{u_1, u_2} velocities, and position $C_{\hat{x}_1, \hat{x}_2}$. All quantities in atomic units.
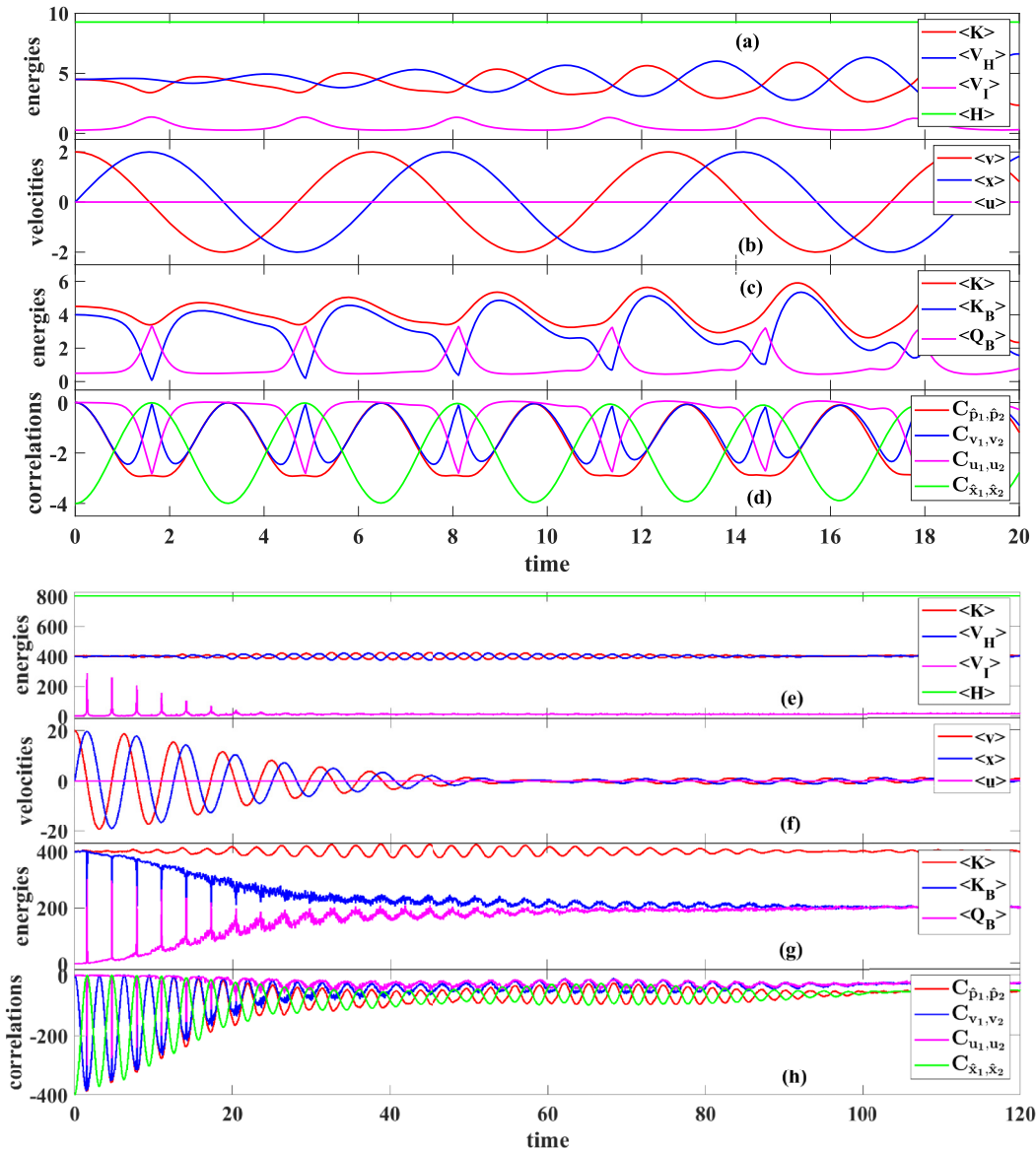
FIG. 3. Expectation values from the dynamics in scenario D3, with mixed x_0, p_0 influence. (a)–(d) A few initial cycles under no disorder with small $(x_{01}, x_{02}) = (-2, 2)$ and small $(p_{01}, p_{02}) = (2, 2)$; (e)–(h) full dynamics under disorder with a large $(x_{01}, x_{02}) = (-20, 20)$ and a large $(p_{01}, p_{02}) = (20, 20)$. (a) and (e) show energies: orthodox kinetic energy $\langle K \rangle$, harmonic confining energy $\langle V_H \rangle$, Coulomb repulsion energy $\langle V_I \rangle$, and total energy $\langle H \rangle$ [$\langle V_I \rangle$ is magnified by 100 in (e)]. (b) and (f) show velocities: Bohmian velocity $\langle v \rangle$, position $\langle x \rangle$, and osmotic velocity $\langle u \rangle$. (c) and (g) show a comparison of the kinetic energies: orthodox $\langle K \rangle$, Bohmian $\langle K_B \rangle$, and quantum potential $\langle Q_B \rangle$ energies. (d) and (h) show correlations: momentum $C_{\hat{p}_1, \hat{p}_2}$, Bohmian C_{v_1, v_2} and osmotic C_{u_1, u_2} velocities, and position $C_{\hat{x}_1, \hat{x}_2}$. All quantities in atomic units.

electrons pass back at $(x_1, x_2) = (-2, 2)$; (iv) at $t = 3\pi/2$ the electrons reach the negative turning point and try to collide at $(x_1, x_2) = (-4, -4)$, with new peaks in $\langle V_I \rangle$ and in $\langle Q_B \rangle$ and again with $\langle K_B \rangle = 0$; and (v) at $t = 2\pi$ the electrons are back to $(x_1, x_2) = (-2, 2)$, and a new cycle starts. The cycle shows that although the initial velocity is the same for both electrons, they acquire different velocities in the dynamics as one moves in favor of and the other against the harmonic potential. The results in Fig. 2(b) are trivially understood from the previous analysis, confirming the center-of-mass character of those quantities: The D2 dynamics, being diagonal in the configuration space $x_1 x_2$, has that $\langle x \rangle$ ranges from $\langle x \rangle = 0$ when electrons are at $(2, -2)$ to $\langle x \rangle = 4$ ($\langle x \rangle = -4$) when

electrons are at the positive (4,4) [negative $(-4, -4)$] turning point, while $\langle v \rangle$ is just out of phase and $\langle u \rangle = 0$ from (22). Interestingly, the correlations in Fig. 2(d) do not change from the D1 dynamics. So let us explain the origin of the double-peak feature in C_{v_1, v_2}: At $t = 0$, $C_{v_1, v_2} = 0$ since both electrons have the same initial velocity to the right; as time evolves, the left (right) electron gains (loses) velocity, therefore negatively increasing C_{v_1, v_2}, which reaches its first peak as the left electron crosses the origin; then the left electron also starts to decrease its velocity until both electrons reach the positive turning point, causing $C_{v_1, v_2} = 0$ at $t = \pi/2$; and finally, electrons then start moving to the left, again with a higher velocity for the left electron, inducing a new negative

increase in C_{v_1, v_2}, until the left electron passes by the origin at its highest velocity, causing the second peak in C_{v_1, v_2}. We remind that such left-right labeling of an electron does not imply that one is "identifying" the electron.

The full D2 dynamics with disorder is seen in Figs. 2(e)–2(h), in which the larger $p_{01} = p_{02} = 20$ induces larger oscillation amplitudes with the same 2π period, except for $\langle V_I \rangle$, which is once more magnified by 100. Overall, the smearing out of the oscillations in $\langle K \rangle$ and $\langle V_H \rangle$, of the peaks in $\langle V_I \rangle$ and $\langle Q_B \rangle$, and of the minima in $\langle K_B \rangle$ happens as the system thermalizes, with such quantities seeming to reach stationary values at $t_{eq} \approx 220$. Thermalization in scenario D2 also induces the feature $\langle x \rangle \approx \langle v \rangle \approx 0$ in Fig. 2(f) [compare with Fig. 1(f)]. All four equations (38)–(41) are also satisfied in scenario D2 at $t > t_{eq}$, such that the virial theorem seems to be restated in Fig. 2(e), and the hidden-variable signature of thermalization is once more seen in Fig. 2(g). While (30) and (42) are also valid in scenario D2, as well as $C_{\hat{p}_1, \hat{p}_2} \approx C_{\hat{x}_1, \hat{x}_2}$, the correlations in Fig. 2(h) become positive (since both electrons move in the same direction) and stabilize at larger magnitudes (from the larger initial velocity).

3. Dynamics from the initial position and the initial velocity

After detailing scenarios D1 and D2 we will only describe here the distinct features of the D3 dynamics. Once more we start from the no-disorder case in Figs. 3(a)–3(d), which has both a small $p_{01} = p_{02} = 2$ and a small $x_{01} = -x_{02} = -2$. Such identical initial values obviously yield $\langle V_H \rangle(0) = \langle K \rangle(0) = 4.5$, and since $\langle V_I \rangle(0) = 0.27$ one has $\langle H \rangle(0) = 9.27$, while $\langle K_B \rangle(0) = 4$ and $\langle Q_B \rangle(0) = 0.5$ are the values building $\langle K \rangle(0)$. The dynamics, though, is more involved since it is a superposition of the two previous scenarios, with cycles in a 2π period. At the initial cycles, $\langle K \rangle$ looks almost constant since $\langle Q_B \rangle$ reaches magnitudes comparable to $\langle K_B \rangle$ [compare Fig. 3(c) with Figs. 2(c) and 1(c)], as $\langle K_B \rangle$ may still vanish whenever $\langle v \rangle = 0$ in Fig. 3(b). The correlation plots in Fig. 3(d), interestingly, are identical to those in Figs. 2(d) and 1(d), while $\langle v \rangle$ and $\langle x \rangle$ in Fig. 3(b) oscillate in between the turning points at $(2,2)$ and $(-2, -2)$, with center-of-mass-like values.

The full D3 dynamics with disorder is shown in Figs. 3(e)–3(h), which considers both a large $p_{01} = p_{02} = 20$ and a large $x_{01} = -x_{02} = -20$. With such values the constancy of the kinetic and potential energies in Fig. 3(e) becomes evident such that, besides the trivial energy conservation in (40), the virial theorem in (41) looks "as if" it is always satisfied at any t, even before thermalization is set at $t_{eq} \approx 110$, mistakenly telling us that some stationary state could be present since $t = 0$. In other words, the onset of thermalization is no longer identifiable in the energy expectation values of Fig. 3(e) (where $\langle V_I \rangle$ is magnified again by 100), although it remains identifiable in Fig. 3(f). The central result of this paper, however, is once more found in Fig. 3(g), where the kinetic energy equipartition in (39) is verified although following a different thermalizing path compared with Figs. 2(g) and 1(g). The correlations in Fig. 3(h) are about the same as in the D1 scenario, where (42), as well as $C_{\hat{p}_1, \hat{p}_2} \approx C_{\hat{x}_1, \hat{x}_2}$, apply once more.

TABLE II. The main expectation values relevant in the discussion of the kinetic energy equipartition, addressed in Figs. 1–3. Expectation values marked with $\times$ cannot directly be computed from a Hermitian operator, but they can be accessed by postprocessing the weak value of the momentum $p_W(\mathbf{x}, t)$.

Expectation	Eq.	Operator	From weak values
$\langle p \rangle$	(20)	$\hat{p}$	$p_W(\mathbf{x}, t)$
$\langle K \rangle$	(28)	$\hat{K}$	$\text{Re}[p_W(\mathbf{x}, t)]^2 + \text{Im}[p_W(\mathbf{x}, t)]^2$
$\langle v \rangle$	(21)	$\times$	$\text{Re}[p_W(\mathbf{x}, t)]$
$\langle u \rangle$	(22)	$\times$	$\text{Im}[p_W(\mathbf{x}, t)]$
$\langle K_B \rangle$	(26)	$\times$	$\text{Re}[p_W(\mathbf{x}, t)]^2$
$\langle Q_B \rangle$	(27)	$\times$	$\text{Im}[p_W(\mathbf{x}, t)]^2$

C. Revisiting the three scenarios within the center-of-mass framework

1. The issue of empirical indistinguishability

All expectation values presented in Figs. 1–3 refer to a single particle, but thanks to the antisymmetry of $\Psi(\mathbf{x}, t)$, there is no need to identify "which" particle. This is true no matter whether they are linked to Hermitian operators such as $\hat{K}$ or $\hat{p}$ or to postprocessings of weak values such as $p_W(\mathbf{x}, t)$, as the exchange symmetry of both the phase and the amplitude of $\Psi(\mathbf{x}, t)$ is directly translated to the current velocity in (3) and the osmotic velocity in (4), respectively (and to the postprocessing data). However, if one is interested in *how* expectation values such as $\langle v \rangle$ or $\langle u \rangle$ are obtained in a laboratory, one needs to differentiate between the ones computed from Hermitian operators and the ones computed from postprocessings of weak values, as indicated in Table II.

Let us illustrate the problem with $N = 2$. The experimental weak value $p_{W,1}(x_1, x_2, t)$ requires two measurements: a first weak measurement linked to $\hat{p}_1$, plus a second strong measurement linked to $\hat{x}_1$ and $\hat{x}_2$. Such a weak value is obtained after a preselection (repeating the same experiment for a large number of identically prepared initial wave functions) plus a postselection (to obtain an ensemble value of all weakly measured momenta whose subsequent strongly measured position yields a specific location); a similar procedure is required for getting $p_{W,2}(x_1, x_2, t)$ by interchanging the measurements on particles 1 and 2. Although $\langle p_{W,1} \rangle = \int dx_1 dx_2 p_{W,1}(x_1, x_2, t)|\Psi(x_1, x_2, t)|^2$ is the same as $\langle p_{W,2} \rangle = \int dx_2 dx_1 p_{W,2}(x_2, x_1, t)|\Psi(x_2, x_1, t)|^2$, their empirical evaluation requires one to identify which are the particles 1 and 2 being weakly or strongly measured, which is impossible for systems with indistinguishable particles. One should keep in mind, though, that while Bohmian particles are ontologically distinguishable, the Bohmian dynamical laws ensure that expectation values are empirically indistinguishable.

To handle this issue, we consider an effective single-particle weak value, $\tilde{p}_{W,j}(x_k, t)$, by defining $\mathbf{X_k} = (x_1, \ldots, x_{k-1}, x_{k+1}, \ldots, x_N)$ such that $\mathbf{x} = (x_k, \mathbf{X_k})$, as

$$\tilde{p}_{W,j}(x_k, t) = \frac{\int d\mathbf{X_k} \, p_{W,j}(x_k, \mathbf{X_k}, t)|\Psi(x_k, \mathbf{X_k}, t)|^2}{P(x_k, t)}, \quad (49)$$

$$P(x_k, t) = \int d\mathbf{X_k} \, |\Psi(x_k, \mathbf{X_k}, t)|^2. \quad (50)$$

It is straightforward to show that

$$\langle \tilde{p}_{W,j} \rangle = \int dx_k \, \tilde{p}_{W,j}(x_k, t) P(x_k, t)$$
$$= \int dx_k d\mathbf{X_k} \, p_{W,j}(x_k, \mathbf{X_k}, t) |\Psi(x_k, \mathbf{X_k}, t)|^2$$
$$= \langle p_{W,j} \rangle. \tag{51}$$

Here, we only need the case $j = k$; the general case $j \neq k$ is found elsewhere [49]. We remind the reader that $\langle \tilde{p}_{W,k} \rangle = \langle p_{W,k} \rangle$ does not imply that $\tilde{p}_{W,k}(x_k, t)$ can promptly be used in place of $p_{W,k}(x_k, \mathbf{X_k}, t)$ to obtain expectation values such as $\langle v \rangle$ or $\langle u \rangle$. This is only the case when the degree x_k is decoupled from the other $N - 1$ degrees in $\mathbf{X_k}$, that is, when one has $\Psi(x_k, \mathbf{X_k}, t) = \psi_k(x_k, t) \psi_{\mathbf{k}}(\mathbf{X_k}, t)$. Then, it is straightforward to show that $p_{W,k}(x_k, \mathbf{X_k}, t) = \tilde{p}_{W,k}(x_k, t)$ with $P(x_k, t) = |\psi_k(x_k, t)|^2$, so that the evaluation of the weak value linked to the weak momentum and position of the particle x_k does not require measurement of the other positions $\mathbf{X_k}$, but it still requires that one identify the particle x_k. This last difficulty can be solved by dealing with the center-of-mass frame.

It is well known [78–83] that our trap Hamiltonian in the absence of the disorder potential $V_D(\mathbf{x})$, that is, when $H(\mathbf{x}) \equiv K(\mathbf{x}) + V_H(\mathbf{x}) + V_I(\mathbf{x})$, can be written in separable terms for center-of-mass coordinates x_c and relative coordinates $\mathbf{X_r} = (x_{r,1}, x_{r,2}, \ldots, x_{r,N-1})$, where $x_c = \sum_{i=1}^{N} x_i / N$ and $x_{r,j} = x_j - x_{j+1}$. In such a situation [Figs. 1(a)–1(d), 2(a)–2(d), and 3(a)–3(d)], the discussion above promptly applies by taking $x_c \equiv x_k$ and $\mathbf{X_r} \equiv \mathbf{X_k}$. Then one indeed could consider $\tilde{p}_{W,c}(x_c, t)$, to which one has experimental access, instead of the intricate $p_{W,c}(x_c, \mathbf{X_r}, t)$ to compute quantities from Table II such as $\tilde{v}_c^2(x_c, t) = \text{Re}(\tilde{p}_{W,c}(x_c, t))^2$ and $\tilde{u}_c^2(x_c, t) = \text{Im}(\tilde{p}_{W,c}(x_c, t))^2$, instead of $v_c^2(x_c, \mathbf{X_r}, t)$ or $u_c^2(x_c, \mathbf{X_r}, t)$. One would also have $H = H_c + H_{\mathbf{r}}$ and $\Psi(x_c, \mathbf{X_r}, t) = \psi_c(x_c, t) \psi_{\mathbf{r}}(\mathbf{X_r}, t)$, such that $\tilde{p}_{W,c}(x_c, t) = p_{W,c}(x_c, \mathbf{X_r}, t)$ in (49) and $P(x_c, t) = |\psi_c(x_c, t)|^2$ in (50). That is, a weak measurement of the momentum of the center of mass followed by a strong measurement of its position, without measuring the other $N - 1$ degrees, should yield information about the N-body trap. The kinetic energy equipartition discussed so far should remain valid in any frame of reference. So the question one needs to pose now is whether or not the inclusion of disorder, which drives the system towards thermalization [Figs. 1(e)–1(h), 2(e)–2(h), and 3(e)–3(h)], induces a coupling between center-of-mass and relative coordinates.

2. Results in the center-of-mass frame

To answer that question, we once more make use of $N = 2$, with $\mathbf{X_r} = (x_{r,1}) \equiv x_r$. The disordered-trap Hamiltonian becomes simply

$$H(x_c, x_r) = H_c(x_c) + H_r(x_r) + V_D(x_c, x_r), \tag{52}$$

with

$$H_c(x_c) = -\frac{1}{4} \frac{\partial^2}{\partial x_c^2} + \omega^2 x_c^2, \tag{53}$$

$$H_r(x_r) = -\frac{\partial^2}{\partial x_r^2} + \frac{1}{4} \omega^2 x_r^2 + \frac{1}{|x_r + \alpha|}; \tag{54}$$

only with $V_D(x_c, x_r) = 0$ would one obtain $\Psi(x_c, x_r, t) = \psi_c(x_c, t) \psi_r(x_r, t)$ with $i \partial \psi_c(x_c, t) / \partial t = H_c \psi_c(x_c, t)$ and $i \partial \psi_r(x_r, t) / \partial t = H_r \psi_r(x_r, t)$. Figure 4 shows the dynamics for scenarios D1, D2, and D3 in the left, middle, and right panels, respectively, in which $\langle V_{H,c} \rangle$ and $\langle K_c \rangle$ ($\langle V_{H,r} \rangle$ and $\langle K_r \rangle$) label the confining potential and kinetic components of (53) [of (54)]; the component related to the Coulomb term $\langle V_{I,r} \rangle$ in (54) is not shown since, as we have seen in Figs. 1–3, it remains small. The labels $\langle K_{B,c} \rangle = \langle (v_1 + v_2)^2 \rangle / 4$ and $\langle K_{B,r} \rangle = \langle (v_1 - v_2)^2 \rangle / 4$ [$\langle Q_{B,c} \rangle = \langle (u_1 + u_2)^2 \rangle / 4$ and $\langle Q_{B,r} \rangle = \langle (u_1 - u_2)^2 \rangle / 4$] for the center-of-mass and relative components, respectively, of the Bohmian kinetic energy (quantum potential energy) are also employed.

Figures 4(a)–4(c) show that indeed, both center-of-mass and relative coordinates thermalize, that is, $\langle V_{H,r} \rangle$ and $\langle K_r \rangle$ on the one hand, while $\langle V_{H,c} \rangle$ and $\langle K_c \rangle$ on the other hand, reach about the same stationary values at the same t_{eq}, with relative energies being larger than the center-of-mass energies in scenarios D1 and D3; the opposite happens in the D2 dynamics, where the relative energies also present a much smaller t_{eq}. The black lines, which present the total energies $E_c = \langle K_c \rangle + \langle V_{H,c} \rangle$ and $E_r = \langle K_r \rangle + \langle V_{H,r} \rangle$, show that, in fact, center-of-mass and relative coordinates are *not* decoupled at $t < t_{eq}$, since their respective energies do not remain constant in the time evolution. So, in principle, the picture presented in Sec. IV C 1 should not apply. However, such energies do stabilize after t_{eq}, seemingly indicating that thermalization implies a negligible dependence of x_c on x_r. This should not come as a surprise since, first, the physics should not be different owing to changing a frame of reference and, second, as the disorder potential is random and does not privilege any degree of freedom, it seems natural to expect that, while coupling is to be found at the beginning, the time evolution should homogeneously spread the probabilities over the configuration space, no matter whether between x_1 and x_2 or x_c and x_r. So, the empirical measurements as pictured in Sec. IV C 1 do apply at thermalization, and more importantly, the negligible dependence of x_c on the relative coordinates becomes an even more robust result for thermalized systems with larger N [84]. Figures 4(d)–4(f) and 4(g)–4(i) confirm that the kinetic energy equipartition remains verified for the center-of-mass and relative coordinates, respectively, for each of the three scenarios, and it should also be verified for any N in this new reference frame. One also has to remember, though, that thermalization has been studied in small systems with as few as six [18], five [6], or two to four bosons [85,86] and even in single-particle systems [87–89].

V. CONCLUSIONS

Weak values have gradually been transitioning from a theoretical curiosity to a practical tool in the laboratory allowing novel characterizations of quantum systems, as they can provide information beyond the traditional expectation values linked to Hermitian operators. In particular, we have shown that weak values of the momentum postselected in positions, without linking the discussion to any specific ontology but reusing the mathematical machinery of both Bohmian and stochastic quantum theories, can be used as a relevant tool to characterize quantum thermalization in closed systems. As
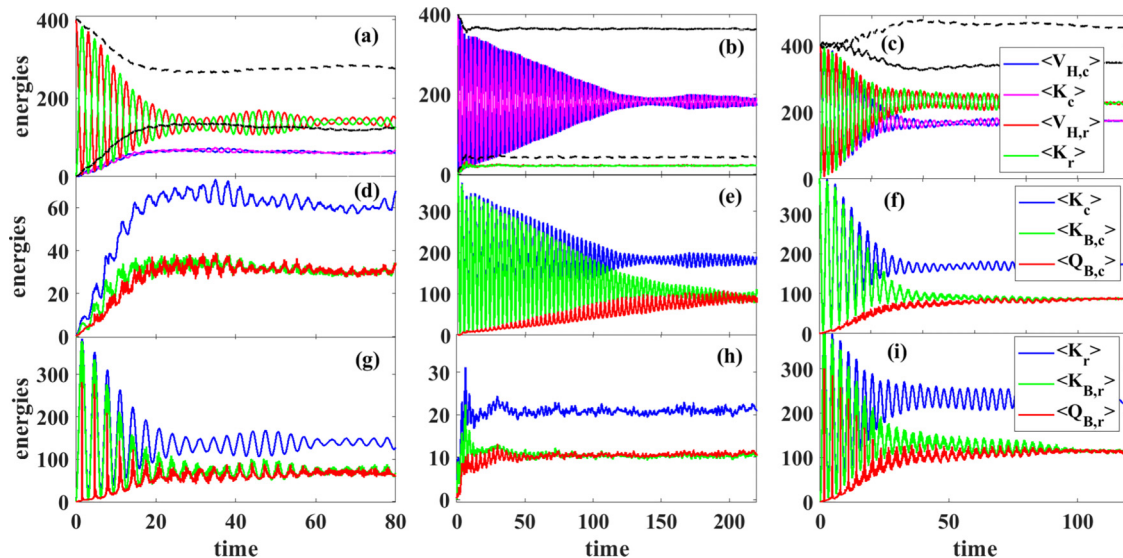
FIG. 4. Center-of-mass and relative energy expectation values for scenarios D1 [(a), (d), and (g)], D2 [(b), (e), and (h)], and D3 [(c), (f), and (i)]. (a)–(c) Kinetic energies $\langle K_c \rangle$ and $\langle K_r \rangle$ and confining potential energies $\langle V_{H,c} \rangle$ and $\langle V_{H,r} \rangle$; the respective total energies $E_c = \langle K_c \rangle + \langle V_{H,c} \rangle$ and $E_r = \langle K_r \rangle + \langle V_{H,r} \rangle$ are shown as black lines. $\langle V_{I,r} \rangle$ is not included. (d)–(f) Bohmian kinetic $\langle K_{B,c} \rangle$ and quantum potential $\langle Q_{B,c} \rangle$ energies in comparison with orthodox $\langle K_c \rangle$ center-of-mass energies. (e)–(h) Bohmian kinetic $\langle K_{B,r} \rangle$ and quantum potential $\langle Q_{B,r} \rangle$ energies in comparison with orthodox $\langle K_r \rangle$ relative energies. The legend in (c) also applies to (a) and (b), the legend in (f) also applies to (d) and (e), and the legend in (i) also applies to (g) and (h). All quantities in atomic units.

an example, we have addressed the monopole oscillations in the configuration space of a two-electron fermionic harmonic trap under random disorder, with different initial conditions employed to initiate three distinct nonequilibrium dynamics.

On the one hand, the expectation values from the orthodox operators cannot always be employed to access the onset of thermalization. For example, $\langle v \rangle$ and $\langle x \rangle$ cannot identify such an onset in Fig. 1(f) for scenario D1, and $\langle K \rangle$ and $\langle V_H \rangle$ cannot identify such an onset in Fig. 3(e) for scenario D3; in scenario D2, both Fig. 2(e) and Fig. 2(f) identify such an onset. The differences between these dynamics and their path to thermalization result from the different initial conditions, in which in the configuration space the dynamics is either antidiagonal (scenario D1), diagonal (scenario D2), or both (scenario D3).

On the other hand, the onset of thermalization is always accessible from its hidden-variable signature in every scenario, *irrespective* of the initial conditions. Not only is (38) obviously satisfied at any time, but also the kinetic energy equipartition in (39), stating that Bohmian kinetic and quantum potential energies should become equal, with each equalizing half of the orthodox kinetic energy, is always true after thermalization is set. This is the same as saying that the squared values of osmotic and current velocities become equal, with each equalizing half of the squared momentum, which also implies that the correlations obey (42) in addition to (30); the validity of (41) in addition to (40) can be taken as a restatement of the virial theorem when reaching some thermalized state.

These hidden variables, linked separately to amplitude (osmotic) and phase (current) components of the many-body wave function, are not linked to orthodox operators, but are accessible in the laboratory through a postprocessing of local-in-position weak-value protocols for momentum and kinetic energy; the real and imaginary parts of the momentum weak

value are tied to the current and osmotic hidden variables, respectively. Thermalization is, so to speak, a manifestation of both real (amplitude) and imaginary (phase) parts of the many-body wave function becoming completely and homogeneously spread through the whole configuration space, making it hard for one to differentiate between them.

In order to properly understand the merits of our work it is essential to notice that all the hidden-variable results in Secs. II and III not only are visualizing tools but also a link between theoretical predictions and empirical data. This link opens unexplored possibilities to characterize static and dynamic properties of quantum systems in the laboratory, being the kinetic energy equipartition studied in this paper just a first example. Notice that the use of the term "hidden variables" has no ontological implication. All quantum theories with empirical agreement with experiments exactly predict the same weak values. In simpler words, the link between theoretical predictions and empirical data does not need to consider any particular ontology. To emphasize the accessibility of weak values in the laboratory, we have also addressed, by moving to the center-of-mass frame of reference, how the weak values of such a center of mass can be employed to approach larger systems with N identical particles, where the kinetic energy equipartition here presented should also be verified.

APPENDIX: EVALUATION OF EXPRESSION (34)

The ensemble value of the product $\langle v_j v_l \rangle$ is

$$
\langle v_j v_l \rangle = \int d\mathbf{x} |\Psi(\mathbf{x},t)|^2 \, v_j(\mathbf{x},t) v_l(\mathbf{x},t) = -\frac{1}{4} \int d\mathbf{x} \frac{1}{|\Psi|^2} (\tilde{\Psi}_j \Psi^* - \tilde{\Psi}_j^* \Psi)(\tilde{\Psi}_l \Psi^* - \tilde{\Psi}_l^* \Psi)
$$

$$
= \frac{1}{2} \int d\mathbf{x} \tilde{\Psi}_j \tilde{\Psi}_l^* - \frac{1}{4} \int d\mathbf{x} \frac{1}{|\Psi|^2} (\tilde{\Psi}_j \Psi^* \tilde{\Psi}_l \Psi^* + \tilde{\Psi}_j^* \Psi \tilde{\Psi}_l^* \Psi). \tag{A1}
$$

Let us evaluate this expression in detail.

1. Evaluation of the term $\frac{1}{2} \int d\mathbf{x} \tilde{\Psi}_j \tilde{\Psi}_l^*$

The first integral of the last line in (A1), using the decomposition $\Psi(\mathbf{x},t) = \sum_n c_n e^{-i\omega_n t} \psi_n(\mathbf{x})$, is rewritten as

$$
\frac{1}{2} \int d\mathbf{x} \Psi_j \tilde{\Psi}_l^* = \frac{1}{2} \sum_{a,b} c_a c_b^* e^{-i(w_a - w_b)t} \int d\mathbf{x} \, \frac{\partial \psi_a(\mathbf{x})}{\partial x_j} \frac{\partial \psi_b^*(\mathbf{x})}{\partial x_l}
$$

$$
= \frac{1}{2} \sum_a |c_a|^2 \int d\mathbf{x} \, \frac{\partial \psi_a(\mathbf{x})}{\partial x_j} \frac{\partial \psi_a^*(\mathbf{x})}{\partial x_l} + \frac{1}{2} \sum_{a \neq b} c_a c_b^* e^{-i(w_a - w_b)t} \int d\mathbf{x} \, \frac{\partial \psi_a(\mathbf{x})}{\partial x_j} \frac{\partial \psi_b^*(\mathbf{x})}{\partial x_l}. \tag{A2}
$$

The first summand (populations or diagonal elements) in (A2) is time independent. For example, for the case $\langle v_j v_j \rangle$, one can rewrite it as

$$
\frac{1}{2} \int d\mathbf{x} \, \frac{\partial \psi_a(\mathbf{x})}{\partial x_j} \frac{\partial \psi_a^*(\mathbf{x})}{\partial x_j} = -\frac{1}{2} \int d\mathbf{x} \, \frac{\partial^2 \psi_a(\mathbf{x})}{\partial x_j^2} \psi_a^*(\mathbf{x}) = \int d\mathbf{x} \, (E_a - V(\mathbf{x})) |\psi_a(\mathbf{x})|^2, \tag{A3}
$$

where we have used that $-\frac{1}{2} \frac{\partial^2 \psi_a(\mathbf{x})}{\partial x_j^2} + V(\mathbf{x})\psi_a(\mathbf{x}) = E_a \psi_a(\mathbf{x})$. Thus

$$
\frac{1}{2} \sum_a |c_a|^2 \int d\mathbf{x} \, \frac{\partial \psi_a(\mathbf{x})}{\partial x_j} \frac{\partial \psi_a^*(\mathbf{x})}{\partial x_l} = \sum_a |c_a|^2 \int d\mathbf{x} \, (E_a - V(\mathbf{x})) |\psi_a(\mathbf{x})|^2, \tag{A4}
$$

such that the first term in (A2) is just the sum of the kinetic energies of the different eigenstates, weighted by the importance of each eigenstate in the description of the initial state, as given by $|c_a|^2$. The relevant point is that its value does not change before or after thermalization.

The second summand (coherences or nondiagonal elements) in (A2) is time dependent, and one can distinguish two contributions:

(i) By defining $c_a = |c_a|e^{i\theta_a}$ and $c_b = |c_b|e^{i\theta_b}$, one can rewrite $c_a c_b^* e^{-i(w_a - w_b)t} = |c_a||c_b|e^{-i((\theta_b - \theta_a)+(w_a - w_b)t)}$. At the initial time $t = 0$, the term $e^{-i((\theta_b - \theta_a)+(w_a - w_b)t)}$ still keeps the initial information θ_a and θ_b, but it becomes basically a random number (with positive or negative real and imaginary parts) as time increases, $(w_a - w_b)t > 2\pi$, giving $e^{-i((\theta_b - \theta_a)+(w_a - w_b)t)} \approx \cos(-(w_a - w_b)t) + i \sin(-(w_a - w_b)t)$. Notice that in the absence of disorder the energy separation of the harmonic potential eigenstates $w_a - w_b$ would be well defined, but disorder randomly modifies the energy spectrum.

(ii) In the absence of disorder, the eigenstates of the harmonic potential have well-defined energies. However, the randomly disordered harmonic potential introduces spatial fluctuation and randomness into the spatial patterns of the a and b eigenstates. As a result, the term $\int d\mathbf{x} \, \frac{\partial \psi_a(\mathbf{x})}{\partial x_j} \frac{\partial \psi_b^*(\mathbf{x})}{\partial x_l}$ for $a \neq b$ becomes basically a random number at the onset of thermalization.

The overall result is that such a second summand in (A2) is basically a sum of random numbers yielding a vanishing contribution. As such, only the time-independent contribution from the first summand in (A2) should remain after the onset of thermalization. The above discussion is the usual explanation of the process of thermalization, and it is directly applicable to any ensemble value of any Hermitian operator. When using the energy eigenstates representation, the expectation value of any Hermitian operator is written as contributions from populations (diagonal elements) and coherences (nondiagonal elements) of the density matrix of the system.

2. Evaluation of the term $\frac{1}{4} \int d\mathbf{x} \frac{1}{|\Psi|^2} (\tilde{\Psi}_j \Psi^* \tilde{\Psi}_l \Psi^*) + \text{c.c.}$

The second integral of the last line in (A1) requires a different explanation because it cannot be written as an expectation value of a Hermitian operator. It is the sum of one component plus its complex conjugate so that it remains indeed real. From

the decomposition $\Psi(\mathbf{x}, t) = \sum_n c_n e^{-i\omega_n t}\psi_n(\mathbf{x})$ it becomes (without the complex-conjugate component for simplicity)

$$
\int d\mathbf{x} \frac{\tilde{\Psi}_j \Psi^* \tilde{\Psi}_l \Psi^*}{|\Psi|^2} = \int d\mathbf{x} \frac{\tilde{\Psi}_j \Psi^* \tilde{\Psi}_l}{\Psi} = \int d\mathbf{x} \frac{\sum_{a,b,c} c_a c_b^* c_c e^{-i w_{a,b,c} t} \tilde{\psi}_{a,j} \psi_b^* \tilde{\psi}_{c,l}}{\sum_{a'} c_{a'} e^{-i w_{a'} t}\psi_{a'}}
$$

$$
= \int d\mathbf{x} \frac{\sum_{w_{a,b,c}=0} c_a c_b^* c_c \tilde{\psi}_{a,j}\psi_b^* \tilde{\psi}_{c,l} + \sum_{w_{a,b,c}\neq 0} c_a c_b^* c_c e^{-i w_{a,b,c} t}\tilde{\psi}_{a,j}\psi_b^*\tilde{\psi}_{c,l}}{\sum_{a'} |c_{a'}|e^{-i(w_{a'}t - \theta_a)}\psi_{a'}}
$$

$$
= \sum_{w_{a,b,c}=0} c_a c_b^* c_c \int d\mathbf{x} \frac{\tilde{\psi}_{a,j}\psi_b^*\tilde{\psi}_{c,l}}{\sum_{a'} |c_{a'}|e^{-i(w_{a'}t - \theta_a)}\psi_{a'}} + \sum_{w_{a,b,c}\neq 0} c_a c_b^* c_c e^{-i w_{a,b,c} t}\int d\mathbf{x}\frac{\tilde{\psi}_{a,j}\psi_b^*\tilde{\psi}_{c,l}}{\sum_{a'}|c_{a'}|e^{-i(w_{a'}t-\theta_a)}\psi_{a'}}, \quad (\text{A5})
$$

where $\tilde{\psi}_{s,q} \equiv \partial\psi_s(\mathbf{x})/\partial x_q$ and $\psi_s \equiv \psi_s(\mathbf{x})$, for $s = a, b, c$, $q = j, l$, and $w_{a,b,c} = w_a - w_b + w_c$. Notice that there is a time-independent term in the numerator of (A5) when $w_{a,b,c} = 0$, but the numerator remains always time dependent and is given, after the equilibration time to eliminate the dependence on θ_a, by $\sum_{a'} |c_{a'}|e^{-i w_{a'} t}\psi_{a'}$. As such, even when the energies of the eigenstates involved in (A5) add to zero, there is no time-independent term. This is the key difference between (A2) and (A5). The rest of the demonstration is about justifying the randomness of the different summands.

As we have discussed for the second summand of (A2), one can distinguish two sources of randomness in (A5):

(i) By defining $c_a = |c_a|e^{i\theta_a}$, $c_b = |c_b|e^{i\theta_b}$, and $c_c = |c_c|e^{i\theta_c}$, one can rewrite $c_a c_b^* c_c e^{-i w_{a,b,c} t} = |c_a||c_b||c_c|e^{-i((-\theta_a + \theta_b - \theta_c) + (w_{a,b,c})t)}$. After the equilibration time, this term in the numerator will become basically a random number. The same will happen for the denominator $e^{-i(\theta_a + (w_a)t)} \approx \cos(-(w_a)t) + i\sin(-(w_a)t)$. As already mentioned, disorder modifies the energy separation of the harmonic potential in a random way.

(ii) In the disordered harmonic potential, the disorder introduces spatial fluctuation and randomness into the spatial patterns of the a, c, and b eigenstates. As a result, the spatial integral of the summand in (A5),

$$
\int d\mathbf{x} \frac{\tilde{\psi}_{a,j}\psi_b^*\tilde{\psi}_{c,l}}{\sum_{a'}|c_{a'}|e^{-i w_{a'} t}\psi_{a'}} = \int d\mathbf{x}\frac{\frac{\partial\psi_a(\mathbf{x})}{\partial x_j}\psi_b^*(\mathbf{x})\frac{\partial\psi_c(\mathbf{x})}{\partial x_l}}{\sum_{a'}|c_{a'}|e^{-i w_{a'} t}\psi_{a'}(\mathbf{x})}, \quad (\text{A6})
$$

becomes basically a random number at the onset of thermalization.

In summary, the whole term in (A5) cannot be separated as the sum of a time-dependent part plus a time-independent part (because there is no time-independent part). Then, the chaotic nature of the eigenstates due to disorder, as explained above, results in (A5) being basically a sum of random numbers yielding a negligible contribution after the onset of thermalization.

[1] M. Ueda, Quantum equilibration, thermalization and prethermalization in ultracold atoms, Nat. Rev. Phys. **2**, 669 (2020).

[2] C. Gogolin and J. Eisert, Equilibration, thermalisation, and the emergence of statistical mechanics in closed quantum systems, Rep. Prog. Phys. **79**, 056001 (2016).

[3] J. Eisert, M. Friesdorf, and C. Gogolin, Quantum many-body systems out of equilibrium, Nat. Phys. **11**, 124 (2015).

[4] V. I. Yukalov, Equilibration and thermalization in finite quantum systems, Laser Phys. Lett. **8**, 485 (2011).

[5] P. Reimann, Transportless equilibration in isolated many-body quantum systems, New J. Phys. **21**, 053014 (2019).

[6] M. Rigol, V. Dunjko, and M. Olshanii, Thermalization and its mechanism for generic isolated quantum systems, Nature (London) **452**, 854 (2008).

[7] R. Nandkishore and D. A. Huse, Many-body localization and thermalization in quantum statistical mechanics, Annu. Rev. Condens. Matter Phys. **6**, 15 (2015).

[8] L. D'Alessio, Y. Kafri, A. Polkovnikov, and M. Rigol, From quantum chaos and eigenstate thermalization to statistical mechanics and thermodynamics, Adv. Phys. **65**, 239 (2016).

[9] J. M. Deutsch, Eigenstate thermalization hypothesis, Rep. Prog. Phys. **81**, 082001 (2018).

[10] T. Langen, R. Geiger, and J. Schmiedmayer, Ultracold atoms out of equilibrium, Annu. Rev. Condens. Matter Phys. **6**, 201 (2015).

[11] M. Lewenstein, A. Sanpera, V. Ahufinger, B. Damski, A. Sen(De), and U. Sen, Ultracold atomic gases in optical lattices: Mimicking condensed matter physics and beyond, Adv. Phys. **56**, 243 (2007).

[12] L. Sanchez-Palencia, D. Clément, P. Lugan, P. Bouyer, and A. Aspect, Disorder-induced trapping versus Anderson localization in Bose–Einstein condensates expanding in disordered potentials, New J. Phys. **10**, 045019 (2008).

[13] A. Polkovnikov, K. Sengupta, A. Silva, and M. Vengalattore, Nonequilibrium dynamics of closed interacting quantum systems, Rev. Mod. Phys. **83**, 863 (2011).

[14] P. Reimann, Eigenstate thermalization: Deutsch's approach and beyond, New J. Phys. **17**, 055025 (2015).

[15] T. R. de Oliveira, C. Charalambous, D. Jonathan, M. Lewenstein, and A. Riera, Equilibration time scales in closed many-body quantum systems, New J. Phys. **20**, 033032 (2018).

[16] T. Kinoshita, T. Wenger, and D. S. Weiss, A quantum Newton's cradle, Nature (London) **440**, 900 (2006).

[17] S. Trotzky, Y.-A. Chen, A. Flesch, I. P. McCulloch, U. Schollwöck, J. Eisert, and I. Bloch, Probing the relaxation towards equilibrium in an isolated strongly correlated one-dimensional Bose gas, Nat. Phys. **8**, 325 (2012).

[18] A. M. Kaufman, M. E. Tai, A. Lukin, M. Rispoli, R. Schittko, P. M. Preiss, and M. Greiner, Quantum thermalization through entanglement in an isolated many-body system, Science **353**, 794 (2016).

[19] J. P. Ronzheimer, M. Schreiber, S. Braun, S. S. Hodgman, S. Langer, I. P. McCulloch, F. Heidrich-Meisner, I. Bloch, and U. Schneider, Expansion Dynamics of Interacting Bosons in Homogeneous Lattices in One and Two Dimensions, Phys. Rev. Lett. **110**, 205301 (2013).

[20] D. Dries, S. E. Pollack, J. M. Hitchcock, and R. G. Hulet, Dissipative transport of a Bose-Einstein condensate, Phys. Rev. A **82**, 033603 (2010).

[21] S. Will, D. Iyer, and M. Rigol, Observation of coherent quench dynamics in a metallic many-body state of fermionic atoms, Nat. Commun. **6**, 6009 (2015).

[22] J. Kajala, F. Massel, and P. Torma, Expansion Dynamics in the One-Dimensional Fermi-Hubbard Model, Phys. Rev. Lett. **106**, 206401 (2011).

[23] U. Schneider, L. Hackermuller, S. Will, Th. Best, I. Bloch, T. A. Costi, R. W. Helmes, D. Rasch, and A. Rosch, Metallic and insulating phases of repulsively interacting fermions in a 3D optical lattice, Science **322**, 1520 (2008).

[24] B. Nagler, K. Jagering, A. Sheikhan, S. Barbosa, J. Koch, S. Eggert, I. Schneider, and A. Widera, Dipole oscillations of fermionic quantum gases along the BEC-BCS crossover in disordered potentials, Phys. Rev. A **101**, 053633 (2020).

[25] U. Schneider, L. Hackermuller, J. P. Ronzheimer, S. Will, S. Braun, T. Best, I. Bloch, E. Demler, S. Mandt, D. Rasch, and A. Rosch, Fermionic transport and out-of-equilibrium dynamics in a homogeneous Hubbard model with ultracold atoms, Nat. Phys. **8**, 213 (2012).

[26] M. Srednicki, Chaos and quantum thermalization, Phys. Rev. E **50**, 888 (1994).

[27] J. M. Deutsch, Quantum statistical mechanics in a closed system, Phys. Rev. A **43**, 2046 (1991).

[28] C. Nation and D. Porras, Taking snapshots of a quantum thermalization process: Emergent classicality in quantum jump trajectories, Phys. Rev. E **102**, 042115 (2020).

[29] M. Rigol, Quantum quenches and thermalization in one-dimensional fermionic systems, Phys. Rev. A **80**, 053607 (2009).

[30] L. F. Santos and M. Rigol, Onset of quantum chaos in one-dimensional bosonic and fermionic systems and its relation to thermalization, Phys. Rev. E **81**, 036206 (2010).

[31] Y. Tang, W. Kao, K.-Y. Li, S. Seo, K. Mallayya, M. Rigol, S. Gopalakrishnan, and B. L. Lev, Thermalization near Integrability in a Dipolar Quantum Newton's Cradle, Phys. Rev. X **8**, 021030 (2018).

[32] C. Gogolin, M. P. Muller, and J. Eisert, Absence of Thermalization in Nonintegrable Systems, Phys. Rev. Lett. **106**, 040401 (2011).

[33] M. Brenes, T. LeBlond, J. Goold, and M. Rigol, Eigenstate Thermalization in a Locally Perturbed Integrable System, Phys. Rev. Lett. **125**, 070605 (2020).

[34] M. Brenes, J. Goold, and M. Rigol, Low-frequency behavior of off-diagonal matrix elements in the integrable XXZ chain and in a locally perturbed quantum-chaotic XXZ chain, Phys. Rev. B **102**, 075127 (2020).

[35] L. de Broglie, Wave mechanics and the atomic structure of matter and radiation, J. Phys. Radium **8**, 225 (1927).

[36] D. Bohm, A suggested interpretation of the quantum theory in terms of "hidden" variables. I, Phys. Rev. **85**, 166 (1952).

[37] E. Nelson, Derivation of the Schrödinger Equation from Newtonian Mechanics, Phys. Rev. **150**, 1079 (1966).

[38] Y. Aharonov, D. Z. Albert, and L. Vaidman, How the Result of a Measurement of a Component of the Spin of a Spin-1/2 Particle can Turn out to be 100, Phys. Rev. Lett. **60**, 1351 (1988).

[39] D. Pandey, R. Sampaio, T. Ala-Nissila, G. Albareda, and X. Oriols, Identifying weak values with intrinsic dynamical properties in modal theories, Phys. Rev. A **103**, 052219 (2021).

[40] H. M. Wiseman, Grounding Bohmian mechanics in weak values and Bayesianism, New J. Phys. **9**, 165 (2007).

[41] D. Dürr, S. Goldstein, and N. Zanghi, On the weak measurement of velocity in Bohmian mechanics, J. Stat. Phys. **134**, 1023 (2009).

[42] D. Marian, N. Zanghi, and X. Oriols, Weak Values from Displacement Currents in Multiterminal Electron Devices, Phys. Rev. Lett. **116**, 110404 (2016).

[43] F. L. Traversa, G. Albareda, M. Di Ventra, and X. Oriols, Robust weak-measurement protocol for Bohmian velocities, Phys. Rev. A **87**, 052124 (2013).

[44] A. Tanaka, Semiclassical theory of weak values, Phys. Lett. A **297**, 307 (2002).

[45] A. Matzkin, Weak values from path integrals, Phys. Rev. Res. **2**, 032048(R) (2020).

[46] S. Kocsis, B. Braverman, S. Ravets, M. J. Stevens, R. P. Mirin, L. K. Shalm, and A. M. Steinberg, Observing the average trajectories of single photons in a two-slit interferometer, Science **332**, 1170 (2011).

[47] A. Hariri, D. Curic, L. Giner, and J. S. Lundeen, Experimental simultaneous readout of the real and imaginary parts of the weak value, Phys. Rev. A **100**, 032119 (2019).

[48] R. Ramos, D. Spierings, I. Racicot, and A. M. Steinberg, Measurement of the time spent by a tunnelling atom within the barrier region, Nature (London) **583**, 529 (2020).

[49] C. F. Destefani and X. Oriols, Assessing quantum thermalization in physical and configuration spaces via many-body weak values, Phys. Rev. A **107**, 012213 (2023).

[50] In this paper, we refer to local-in-position weak values as the weak values constructed by the weak measurement of a property (typically the momentum of the system) and a posterior postselection by the strong measurement of the position. The typical example of such a weak value is the measurement of Bohmian velocities [39]. Such a weak value will also be referred to as the weak value of the momentum postselected by the position. Notice that such weak values of the momentum postselected in position are not the weak values of the position that have been addressed in semiclassical theories and quantum chaos [44,45].

[51] A. Valdes-Hernandez, L. de la Peña, and A. M. Cetto, Strong entanglement criterion involving momentum weak values, Phys. Lett. A **383**, 838 (2019).

[52] A. G. Kofman, S. Ashhab, and F. Nori, Nonperturbative theory of weak pre- and post-selected measurements, Phys. Rep. **520**, 43 (2012).

[53] J. Dressel, M. Malik, F. M. Miatto, A. N. Jordan, and R. W. Boyd, Understanding quantum weak values: Basics and applications, Rev. Mod. Phys. **86**, 307 (2014).

[54] K. Renziehausen and I. Barth, The connection between Bohmian mechanics and many-particle quantum hydrodynamics, Found. Phys. **50**, 772 (2020).

[55] O. A. Castro-Alvaredo, B. Doyon, and T. Yoshimura, Emergent Hydrodynamics in Integrable Quantum Systems Out of Equilibrium, Phys. Rev. X **6**, 041065 (2016).

[56] V. Alba, B. Bertini, M. Fagotti, L. Piroli, and P. Ruggiero, Generalized-hydrodynamic approach to inhomogeneous quenches: Correlations, entanglement and quantum effects, J. Stat. Mech. (2021) 114004.

[57] I. Bouchoule and J. Dubail, Generalized hydrodynamics in the one-dimensional Bose gas: Theory and experiments, J. Stat. Mech. (2022) 014003.

[58] X. Oriols and J. Mompart, *Applied Bohmian Mechanics: From Nanoscale Systems to Cosmology* (Pan Stanford, Singapore, 2012).

[59] A. O. T. Pang, H. Ferretti, N. Lupu-Gladstein, W.-K. Tham, A. Brodutch, K. Bonsma-Fisher, J. E. Sipe, and A. M. Steinberg, Experimental comparison of Bohm-like theories with different primary ontologies, Quantum **4**, 365 (2020).

[60] J. S. Lundeen, B. Sutherland, A. Patel, C. Stewart, and C. Bamber, Direct measurement of the quantum wavefunction, Nature (London) **474**, 188 (2011).

[61] J. Dressel and A. N. Jordan, Significance of the imaginary part of the weak value, Phys. Rev. A **85**, 012107 (2012).

[62] E. Cohen and E. Pollak, Determination of weak values of quantum operators using only strong measurements, Phys. Rev. A **98**, 042112 (2018).

[63] G. Dennis, M. A. de Gosson, and B. J. Hiley, Bohm's quantum potential as an internal energy, Phys. Lett. A **379**, 1224 (2015).

[64] E. Heifetz and E. Cohen, Toward a thermo-hydrodynamic like description of Schrödinger equation via the Madelung formulation and Fisher information, Found. Phys. **45**, 1514 (2015).

[65] G. Grössing, On the thermodynamic origin of the quantum potential, Phys. A (Amsterdam) **388**, 811 (2009).

[66] A. S. Sanz, Bohm's approach to quantum mechanics: Alternative theory or practical picture?, Front. Phys. **14**, 11301 (2019).

[67] B. J. Hiley, Weak values: Approach through the Clifford and Moyal algebras, J. Phys.: Conf. Ser. **361**, 012014 (2012).

[68] R. Flack and B. J. Hiley, Feynman paths and weak values, Entropy **20**, 367 (2018).

[69] Notice that the sum in Eq. (32) is over the number of eigenstates $|n\rangle$ (not the number of particles). The argumentation about thermalization is related to the absence of correlation between the eigenstates $|n\rangle$ and $|m\rangle$ for $n \neq m$ at the onset of thermalization, when the terms $a_{m,n} = \langle m|\hat{a}|n\rangle$ and $\rho_{n,m}(t) = c_m^* c_n e^{i(\omega_m - \omega_n)t}$ are expected to become essentially random numbers. As a result, the sum of these positive and negative nondiagonal elements in Eq. (32) should become negligible for times larger than the thermalization time. While a large number of particles can help ensure the lack of correlation among eigenstates, strictly speaking, the above argument can equivalently be applied to single- or many-particle systems as long as the absence of correlation is guaranteed.

[70] Y.-W. Hsueh, C.-H. Hsueh, and W.-C. Wu, Thermalization in a quantum harmonic oscillator with random disorder, Entropy **22**, 855 (2020).

[71] L. Pezze, B. Hambrecht, and L. Sanchez-Palencia, Dipole oscillations of a Fermi gas in a disordered trap: Damping and localization, Europhys. Lett. **88**, 30009 (2009).

[72] L. Pezze and L. Sanchez-Palencia, Localized and Extended States in a Disordered Trap, Phys. Rev. Lett. **106**, 040601 (2011).

[73] C.-H. Hsueh, R. Ong, J.-F. Tseng, M. Tsubota, and W.-C. Wu, Thermalization and localization of an oscillating Bose-Einstein

[74] R. Ong, C.-H. Hsueh, and W.-C. Wu, Anderson localization in an oscillating Rydberg-dressed condensate with random disorder, Phys. Rev. A **100**, 053619 (2019).

[75] D. Clément, A. F. Varón, J. A. Retter, L. Sanchez-Palencia, A. Aspect, and P. Bouyer, Experimental study of the transport of coherent interacting matter-waves in a 1D random potential induced by laser speckle, New J. Phys. **8**, 165 (2006).

[76] J. Billy, V. Josse, Z. Zuo, A. Bernard, B. Hambrecht, P. Lugan, D. Clément, L. Sanchez-Palencia, P. Bouyer, and A. Aspect, Direct observation of Anderson localization of matter waves in a controlled disorder, Nature (London) **453**, 891 (2008).

[77] All figures in this paper consider $\omega = 1.0$, $\alpha = 0.01$, $\sigma_1 = \sigma_2 = 1/\sqrt{\omega} = 1.0$, $\gamma_D = 25$, and $\sigma_D \approx \Delta x$, with Δx being the position resolution of the grid, defined in such a way that its momentum resolution is $\Delta p \approx \Delta x$. The initial wave packet is antisymmetrized, such that the label j in quantities such as $\langle x_{1,2} \rangle$ is redundant. The final simulation time is $t_f = 100$ for scenario D1, $t_f = 250$ for scenario D2, and $t_f = 150$ for scenario D3, with time step $\Delta t = 0.001$. Simulation boxes are $[-60, 60]$ with 2048 points for each degree of freedom in the configuration space $x_1 x_2$, so that for $N = 2$ its size is $\approx 4 \times 10^6$.

[78] J. W. Abraham, K. Balzer, D. Hochstuhl, and M. Bonitz, Quantum breathing mode of interacting particles in a one-dimensional harmonic trap, Phys. Rev. B **86**, 125112 (2012).

[79] C. R. McDonald, G. Orlando, J. W. Abraham, D. Hochstuhl, M. Bonitz, and T. Brabec, Theory of the Quantum Breathing Mode in Harmonic Traps and its Use as a Diagnostic Tool, Phys. Rev. Lett. **111**, 256801 (2013).

[80] J. W. Abraham, M. Bonitz, C. McDonald, G. Orlando, and T. Brabec, Quantum breathing mode of trapped systems in one and two dimensions, New J. Phys. **16**, 013001 (2014).

[81] S. Bauch, K. Balzer, C. Henning, and M. Bonitz, Quantum breathing mode of trapped bosons and fermions at arbitrary coupling, Phys. Rev. B **80**, 054515 (2009).

[82] M. Taut, Two electrons in an external oscillator potential: Particular analytic solutions of a Coulomb correlation problem, Phys. Rev. A **48**, 3561 (1993).

[83] S. Mandal, P. K. Mukherjee, and G. H. F. Diercksen, Two electrons in a harmonic potential: An approximate analytical solution, J. Phys. B: At. Mol. Opt. Phys. **36**, 4483 (2003).

[84] X. Oriols and A. Benseny, Conditions for the classicality of the center of mass of many-particle quantum states, New J. Phys. **19**, 063031 (2017).

[85] T. Fogarty, M. Á. García-March, L. F. Santos, and N. L. Harshman, Probing the edge between integrability and quantum chaos in interacting few-atom systems, Quantum **5**, 486 (2021).

[86] G. Zisling, L. F. Santos, and Y. B. Lev, How many particles make up a chaotic many-body quantum system?, SciPost Phys. **10**, 088 (2021).

[87] Md. M. Ali, W.-M. Huang, and W.-M. Zhang, Quantum thermodynamics of single particle systems, Sci. Rep. **10**, 13500 (2020).

[88] J.-Q. Liao, H. Dong, and C. P. Sun, Single-particle machine for quantum thermalization, Phys. Rev. A **81**, 052121 (2010).

[89] P. Łydżba, Y. Zhang, M. Rigol, and L. Vidmar, Single-particle eigenstate thermalization in quantum-chaotic quadratic Hamiltonians, Phys. Rev. B **104**, 214203 (2021).